Inorganic Chemistry

Article

pubs.acs.org/IC

Syntheses and Luminescent Properties of 3,5-Diphenylpyrazolato-Bridged Heteropolynuclear Platinum Complexes. The Influence of Chloride Ligands on the Emission Energy Revealed by the Systematic Replacement of Chloride Ligands by 3,5-Dimethylpyrazolate

Seiji Akatsu,[†] Yasunori Kanematsu,[†] Taka-aki Kurihara,[†] Shota Sueyoshi,[†] Yasuhiro Arikawa,[†] Masayoshi Onishi,[†] Shoji Ishizaka,[‡] Noboru Kitamura,[§] Yoshihide Nakao,[¶,⊥] Shigeyoshi Sakaki,[¶] and Keisuke Umakoshi*[,†]

[†]Division of Chemistry and Materials Science, Graduate School of Engineering, Nagasaki University, Bunkyo-machi, Nagasaki 852-8521, Japan

[‡]Department of Chemistry, Graduate School of Science, Hiroshima University, Kagamiyama, Higashi-Hiroshima, 739-8526, Japan

[§]Division of Chemistry, Graduate School of Science, Hokkaido University, Kita-ku, Sapporo 060-0810, Japan

[¶]Fukui Institute for Fundamental Chemistry, Kyoto University, Takano-Nishihiraki-cho, Sakyou-ku, Kyoto 606-8103, Japan

[⊥]Department of Molecular Engineering, Graduate School of Engineering, Kyoto University, Kyoto-Daigaku-Katsura, Nishikyou-ku, Kyoto 615-8510, Japan

Supporting Information

ABSTRACT: Heteropolynuclear Pt^{II} complexes with 3,5-diphenylpyrazolate $[Pt_2Ag_4(\mu\text{-}Cl)_2(\mu\text{-}Ph_2pz)_6]$ (**3**), $[Pt_2Ag_2Cl_2(\mu\text{-}Ph_2pz)_4(Ph_2pzH)_2]$ (**4**), $[Pt_2Cu_2Cl_2(\mu\text{-}Ph_2pz)_4(Ph_2pzH)_2]$ (**5**), $[Pt_2Ag_4(\mu\text{-}Cl)(\mu\text{-}Me_2pz)(\mu\text{-}Ph_2pz)_6]$ (**7**), and $[Pt_2Ag_4(\mu\text{-}Me_2pz)_2(\mu\text{-}Ph_2pz)_6]$ (**8**) have been prepared and structurally characterized. These complexes are luminescent except for **5** in the solid state at an ambient temperature with emissions of red-orange (**3**), orange (**4**), yellow-orange (**7**), and green (**8**) light, respectively. Systematic red shift of the emission energies with the number of chloride ligands was observed for **3**, **7**, and **8**. DFT calculations indicate that the highest occupied molecular orbital (HOMO) as well as HOMO-1 of the heterohexanuclear complexes, **3**, **7**, and **8**, having Pt_2Ag_4 core, mainly consist of $d\delta$ orbital of Pt^{II} and π orbitals of Ph_2pz ligands, while the lowest unoccupied molecular orbital (LUMO) of these complexes mainly consists of in-phase combination of 6p of two Pt^{II} centers and 5p of four Ag^{I} centers. It is likely that the emissions of **3**, **7**, and **8** are attributed to emissive states derived from the $Pt_2(d)/\pi \rightarrow Pt_2Ag_4$ transitions, the emission energy of which depends on the ratio of chloride ligands to pyrazolate ligands.

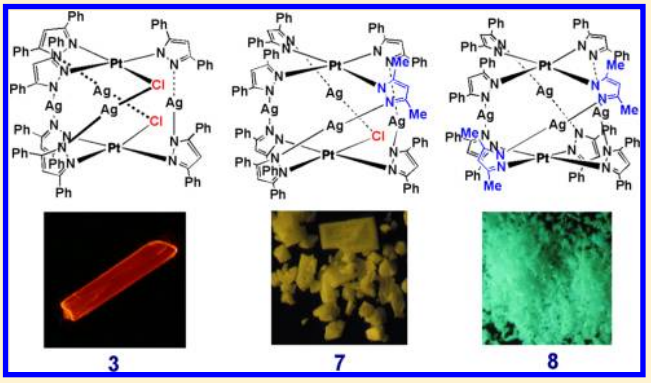

INTRODUCTION

Heteropolynuclear transition-metal complexes have been attracting much attention because they are expected to exhibit characteristic interactions and cooperative effects between the transition elements and provide novel functions that cannot be obtainable by one kind transition metal element. The syntheses of heterohexanuclear Pt^{II} complexes $[Pt_2M_4(C{\equiv}CR)_8]$ (M^{I} = Cu^{I}, Ag^{I}, Au^{I}; R = *t*-butyl, phenyl)[1] have prompted studies on the photophysical properties of these mixed-metal complexes containing group 11 metal ions[2−11] and related complexes containing main group metal ions (Cd^{II}, Tl^{I}, Pb^{II}),[10−18] as well as lanthanide ions.[19−25] Heterohexanuclear Pt^{II} complexes stabilized by both of alkynyl and 3,5-dimethylpyrazolate (Me_2pz) have also been prepared.[6] We have also prepared brightly luminescent heterohexanuclear Pt^{II} complexes $[Pt_2M_4(\mu\text{-}Me_2pz)_8]$ (M^{I} = Ag^{I}, Cu^{I}) by using only 3,5-dimethylpyrazolate as bridging ligands instead of alkynyl ligands.[26] Furthermore, we have succeeded in the preparation of heterohexanuclear Pt^{II} complexes $[Pt_2Au_2M_2(\mu\text{-}Me_2pz)_8]$ (M^{I} = Ag^{I}, Cu^{I}) and achieved the fine-tuning of the emission energy by incorporating the third transition metal element such as Ag^{I} and Cu^{I}.[27] These heterohexanuclear Pt^{II} complexes exhibit colorful luminescence. Large difference of emission energy was observed depending on the nature of the coinage metal ions (Cu, Ag, or Au) among these complexes. The low

Received: December 10, 2011

   dx.doi.org/10.1021/ic202663q | Inorg. Chem. XXXX, XXX, XXX−XXX

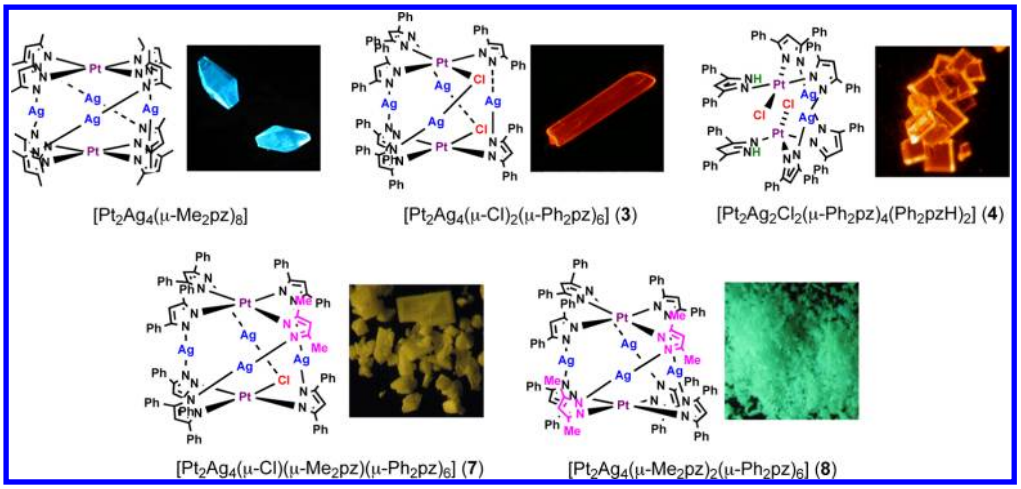

Figure 1. Schematic representation of Pt_2Ag_4 and Pt_2Ag_2 complexes with photographs showing their luminescence in the solid state upon exposure to UV radiation at an ambient temperature.

energy emission was assigned to a metal−ligand-to-metal charge transfer (^{3}MLM′CT) transition (Pt(d)π(C≡CR) → Pt(p_z)/M′(sp)/π*(C≡CR)) modified by Pt···M′ and M′···M′ contact for $[Pt_2M_4(C{\equiv}CR)_8]$.[5−7] Similarly the low energy emissions of dimethylpyrazolato-bridged complexes $[Pt_2M_4(\mu\text{-}Me_2pz)_8]$ were assigned to the transition from the in-phase combination of 6p(Pt) and 5p(Ag) to the dδ(Pt) nonbonding orbitals ($^3[Pt_2 \rightarrow Pt_2Ag_4]$) for M = Ag and the transition from the in-phase combination of 6p(Pt) and 4p(Cu) orbitals to a dπ(Cu) orbital localized on one of the four Cu ions ($^3[Cu(d) \rightarrow Pt_2Cu_4]$) for M = Cu, respectively, reflecting the difference in d orbital energies of Pt, Ag, and Cu.[26] These assignments indicate that the emissions of $[Pt_2M_4(C{\equiv}CR)_8]$ and $[Pt_2M_4(\mu\text{-}Me_2pz)_8]$ occur from the excited state containing one-electron transition from Pt(d) (or Cu(d)) orbital to the in-phase combination among coinage metal ions and Pt^{II} ions.

The Pt_2Ag_4 complexes with 3,5-dialkylpyrazolates (R_2pz), $[Pt_2Ag_4(\mu\text{-}R_2pz)_8]$, exhibit sky-blue to green emission.[26] The use of 3,5-diphenylpyrazole (Ph_2pzH) as a bridging ligand instead of alkylpyrazoles, on the other hand, afforded $[Pt_2Ag_4(\mu\text{-}Cl)_2(\mu\text{-}Ph_2pz)_6]$ (**3**) containing two μ-chloro ligands in the complex molecule. It is very interesting that **3** exhibits red-orange luminescence in the solid state upon exposure to UV radiation in spite of the presence of octahedral Pt_2Ag_4 core unlike $[Pt_2Ag_4(\mu\text{-}R_2pz)_8]$ (Figure 1). To the best of our knowledge, however, very little is discussed about the dependence of the emission energy on the molecular structure of Pt_2M_4 core. It is thus of considerable interest to elucidate the origin of such large difference of emission energies between $[Pt_2Ag_4(\mu\text{-}Me_2pz)_8]$ and **3**. Furthermore we have also succeeded in the replacement of chloride ligand in chlorotris(3,5-diphenylpyrazole) complex with 3,5-dimethylpyrazole, which leads to the synthesis of chloride-free Pt_2Ag_4 complex bridged by Ph_2pz and Me_2pz. Thus, one can expect that the complexes bearing Pt_2Ag_4 core provide new findings about the relation between the molecular structure of the Pt_2Ag_4 core and the emission spectra.

In this paper, we wish to report the syntheses, structures, and photophysical properties of dichloro-, monochloro-, and chloride-free Pt_2Ag_4 complexes of 3,5-diphenylpyrazolate, as well as their precursor mononuclear Pt^{II} complexes, and dichloro-Pt_2Ag_2 and Pt_2Cu_2 complexes. Our purposes here are to clarify the dependence of emission energy on the molecular structure and to elucidate the reasons.

RESULTS AND DISCUSSION

Preparation of Complexes. It is known that the pK_a value of the conjugate acid of 3,5-dimethylpyrazole (Me_2pzH; 4.06) is higher than that of nonsubstituted pyrazole (pzH; 2.83) as shown in Figure 2.[28] On the contrary, the corresponding value

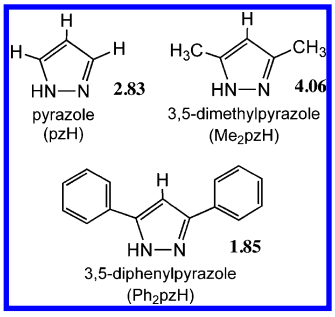

Figure 2. p*K*a values of conjugate acid of pyrazole, 3,5-dimethylpyrazole, and 3,5-diphenylpyrazole.

of Ph_2pzH (1.85) is smaller than that of pzH, indicating that the coordination ability of Ph_2pzH is weaker than those of Me_2pzH and pzH. Actually the reactions of Pt^{II} starting material, $[PtCl_2(C_2H_5CN)_2]$, with Me_2pzH and pzH afford tetrakis(pyrazole derivative) complexes, $[Pt(Me_2pzH)_4]Cl_2$ and $[Pt(pzH)_4]Cl_2$, respectively. However, as mentioned below, the reaction with Ph_2pzH affords chlorotris(3,5-diphenylpyrazole) complex, $[PtCl(Ph_2pzH)_3]Cl$ (**1**), which contains an unsubstituted chloride ligand in the complex cation (Scheme 1). The effect of the basicity of pyrazole derivatives on the geometrical structure and reactivity of product has not been fully understood. We have now found the geometrical preference of mononuclear Pt^{II} complexes of pyrazole derivatives, which gives the guideline for the synthesis of tetrakis(pyrazole derivative) complexes and chlorotris(pyrazole derivative) complex.

The reaction of $[PtCl_2(C_2H_5CN)_2]$ with 3,5-diphenylpyrazole (Ph_2pzH) afforded a cationic mononuclear platinum complex, $[PtCl(Ph_2pzH)_3]Cl$ (**1**), in which a chloride ligand and three neutral Ph_2pzH ligands coordinate to the Pt^{II} ion in a

dx.doi.org/10.1021/ic202663q | Inorg. Chem. XXXX, XXX, XXX−XXX

Scheme 1. Geometrical Preference of Mononuclear Platinum Complexes

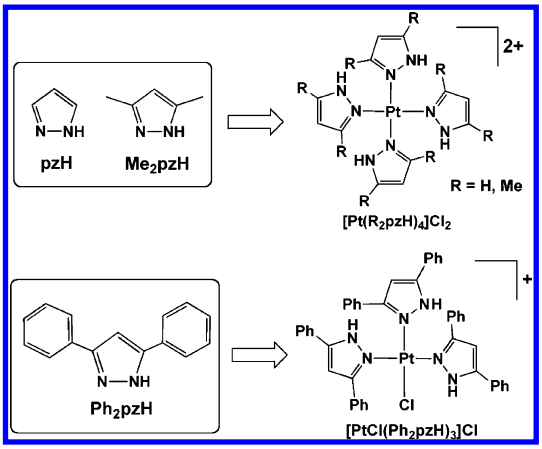

monodentate fashion, probably due to weaker basicity of Ph_2pzH (Scheme 2). A treatment of **1** with strong base brought about liberation of a proton from one of the three Ph_2pzH ligands as well as loss of an outer sphere chloride ligand to give a neutral mononuclear complex $[PtCl(Ph_2pz)(Ph_2pzH)_2]$ (**2**), which is stabilized by an intramolecular hydrogen bonding. This is different from the formation of dimer complex $[\{Pt(Me_2pz)_2(Me_2pzH)_2\}_2]$ stabilized by intermolecular hydrogen bonding, upon treatment of a cationic mononuclear complex $[Pt(Me_2pzH)_4]Cl_2$ with base.[26] The preference of the formation of mononuclear complex and dimer complex seems to be associated with the bulkiness of substituent groups on the pyrazoles. The reaction of the neutral mononuclear complex with Ag^I ion afforded a di(μ-chloro) complex, $[Pt_2Ag_4(\mu\text{-}Cl)_2(\mu\text{-}Ph_2pz)_6]$ (**3**), which consists of two Pt^{II} ions, four Ag^I ions, two chloride ligands, and six Ph_2pz ligands. The complex **3** exhibits red-orange emission in the solid state upon exposure to UV radiation at an ambient temperature.

It also became obvious that **3** can be prepared in a stepwise manner via $[Pt_2Ag_2Cl_2(\mu\text{-}Ph_2pz)_4(Ph_2pzH)_2]$ (**4**), which exhibits orange emission in the solid state. Although the $Pt_2Ag_2Cl_2$ complex **4** was obtained even by the reaction of neutral mononuclear complex **2** with an excess amount of $AgBF_4$ in the absence of Et_3N, the reaction of **2** with $AgBF_4$ in a 1:1 ratio gave **4** and that in a 1:2 ratio gave **3**, respectively, in the presence of Et_3N in good yield. Furthermore, similarly to the reaction of **2** with Ag^I ion, that with Cu^I ion also gave corresponding $Pt_2Cu_2Cl_2$ complex, $[Pt_2Cu_2Cl_2(\mu\text{-}Ph_2pz)_4(Ph_2pzH)_2]$ (**5**).

In order to elucidate, from the viewpoint of synthetic chemistry, whether the main factor of lower energy emission (red-orange emission) of **3** is the coordination of chloride ligand to Pt atom or not, we have also conducted the replacement of chloride ligands in **3** with Me_2pz, which can be regarded as a stronger base than Ph_2pz (Figure 2). The chloride ligand in the neutral complex **2**, as well as cationic complex **1**, could not be replaced by Ph_2pz anion. However the reaction of **1** with Me_2pzH in the presence of Et_3N partially proceeded to give an intermediate species, which is mainly consisting of $[Pt(Ph_2pz)_2(Me_2pzH)(Ph_2pzH)]$ (**6**, vide infra) and **2** (see Supporting Information). Further reaction of the intermediate species with $AgBF_4$ afforded a (μ-chloro)(μ-dimethylpyrazolato) complex, $[Pt_2Ag_4(\mu\text{-}Cl)(\mu\text{-}Me_2pz)(\mu\text{-}Ph_2pz)_6]$ (**7**), which exhibits yellow-orange emission in the solid state (Figure 1). It is noteworthy here that the three-component reaction of isolated **2**, isolated **6**, and $AgBF_4$ gave **7** in much better yield.

Since it was found that the reaction of cationic complex **1** with Me_2pzH even in the presence of Et_3N does not give a chloride-free mononuclear complex as a major product, next we attempted to replace the chloride ligand with Me_2pzH by using neutral complex **2**. Fortunately the reaction of **2** with potassium salt of 3,5-dimethylpyrazole ($K[Me_2pz]$) afforded a neutral chloride-free complex **6** as expected. Finally the reaction of **6** with Ag^I ion gave a chloride-free Pt_2Ag_4 complex, $[Pt_2Ag_4(\mu\text{-}Me_2pz)_2(\mu\text{-}Ph_2pz)_6]$ (**8**), which exhibits green emission in the solid state (Figure 1). Thus it can be concluded from the preparation of monochloro and chloride-free Pt_2Ag_4 complexes that the lower energy shift of the emission spectrum (vide infra) in **3** mainly originates from the coordination of chloride ligands to Pt atoms.

Crystal Structures. X-ray structural analyses of **2**·CH_3OH, **3**·$3CH_2Cl_2$, **4**·$2CH_3CN$, **5**·CH_3CN, **7**·$0.5CH_3OH$·$0.5H_2O$, and **8** were performed. Although cluster complexes **3**, **4**, **5**, and **7** crystallized with solvent molecules, any contacts between cluster complexes with solvent molecules were not found in their crystal structures (Supporting Information Figures S14–S17).

The neutral mononuclear platinum complex with 3,5-diphenylpyrazole, $[PtCl(Ph_2pz)(Ph_2pzH)_2]$ (**2**), which is the precursor of **3**, **4**, **5**, **6**, and **7**, crystallized with a methanol molecule as a solvent of crystallization. The molecular structure of **2** is shown in Figure 3. The complex **2** has a structure in which a chloride ion, a Ph_2pz anion and two neutral Ph_2pzH ligands coordinate to the Pt^{II} center. One of the two Ph_2pzH ligands forms intramolecular hydrogen bonding (N12–H12···N22) together with the Ph_2pz ligand (Supporting Information Table S1). The other Ph_2pzH ligand also forms hydrogen bonding (N32–H32···O1) with methanol molecule. These two hydrogen atoms participating in the hydrogen bonding were found from the Fourier map and refined isotropically in the structural analysis.

The di(μ-chloro) complex, $[Pt_2Ag_4(\mu\text{-}Cl)_2(\mu\text{-}Ph_2pz)_6]$ (**3**), crystallizes with three dichloromethane molecules, and the molecular structure of **3** is shown in Figure 4. The complex molecule is formed by liberation of four protons in total from two molecules of **2** and incorporation of four Ag^I ions into the molecule. A chloride ion and three Ph_2pz anions coordinate to each Pt^{II} center to form $\{PtCl(Ph_2pz)_3\}$ unit, and four Ag^I ions are sandwiched by the two $\{PtCl(Ph_2pz)_3\}$ units, each Ag^I ion being located between two Ph_2pz ligands and between chloride ligand and Ph_2pz ligand. The chloride ligands act as bridging ligands in **3**, and the Pt_2Ag_4 core can be regarded as a distorted octahedron similarly to $[Pt_2Ag_4(\mu\text{-}Me_2pz)_8]$.[26] The complex molecule has an idealized 2-fold axis passing through Ag3 and Ag4. The Pt···Pt distance in **3** is 5.0276(8) Å (Supporting Information Table S2). The Pt···Ag distances are ranging from 3.0069(9) to 3.5337(8) Å, and the proximate Ag···Ag distances are ranging from 2.9647(13) to 3.3367(13) Å. The Pt–Cl distances (2.337(3) and 2.3379(19) Å) in **3** are ca. 0.04 Å longer than those in the precursor complex **2** (2.299(2) Å), $|\{[(PPh_3)(C_6F_5)Pt(\mu\text{-}Cl)]_2Ag\}(\mu\text{-}Cl)_2Ag(MeOH)|_n$ (**9**) (2.295(4), 2.308(3) Å),[29] and $[(Me)(N{-}N)Pt(\mu\text{-}Cl)Ag(\mu\text{-}Cl)Pt(N{-}N)(Me)]BF_4$ (N–N = ArN=C(Me)C(Me)=NAr, Ar = 2,6-(^{i}Pr)$_2$C$_6$H$_3$) (**10**) (2.291(1), 2.298(1) Å).[30] The Ag–Cl distances (2.486(3) and 2.518(3) Å) in **3** fall into the range of Ag–Cl distances found in **9** (2.225(5), 2.400(6), 2.551(3)

dx.doi.org/10.1021/ic202663q | Inorg. Chem. XXXX, XXX, XXX–XXX

Scheme 2. Preparative Methods for 3, 7, and 8

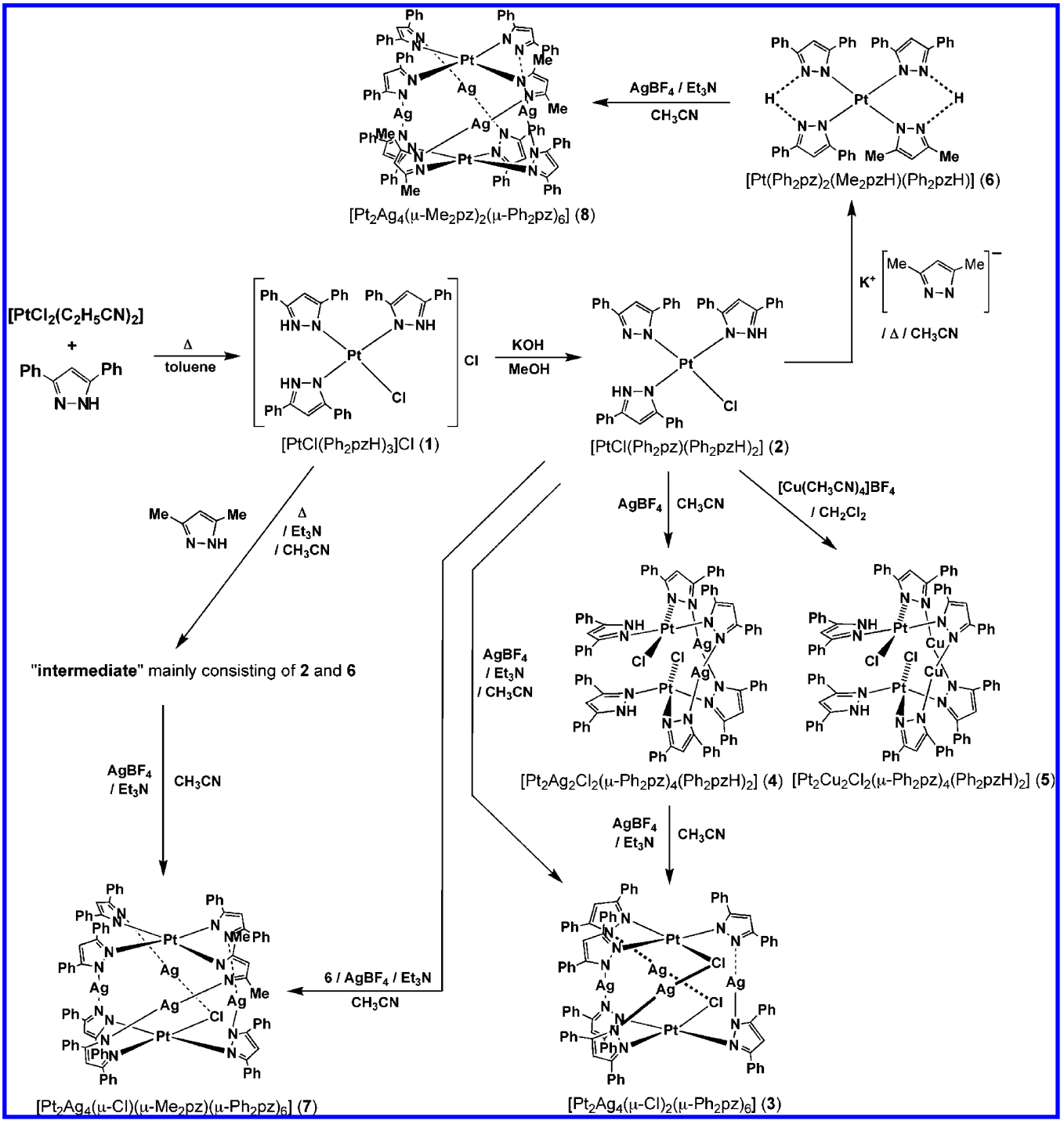

Å)[29] and in **10** (2.398(1), 2.471(1) Å).[30] The Ag−Cl distance seems to be readily changed by alterations in Pt−Cl−Ag angle.

$[Pt_2Ag_2Cl_2(\mu\text{-}Ph_2pz)_4(Ph_2pzH)_2]$ (**4**) crystallizes with two acetonitrile molecules, and the molecular structure of **4** is shown in Figure 5. The complex molecule is formed by liberation of two protons in total from two molecules of **2** and incorporation of two Ag^I ions into the molecule. A chloride ion, two Ph_2pz anions and a neutral Ph_2pzH molecule coordinate to each Pt^{II} center, and each Ag^I ion is located between the two Ph_2pz ligands. The complex molecule has a crystallographically imposed 2-fold axis passing through the midpoint of Pt1···Pt1* and the midpoint of Ag1···Ag1*, and half of the atoms in the molecule are independent. The Pt···Pt distance in **4** is 4.2846(3) Å, which is ~0.75 Å shorter than that in **3** (Supporting Information Table S3). The Pt···Ag distances (3.2156(5) and 3.4554(4) Å) and the Ag···Ag distance (3.1111(6) Å) in **4** are comparable to those in **3**, respectively. The Pt−Cl distance in **4** (2.3303(12) Å) is also comparable to that in **3**.[31]

The copper analogue, $[Pt_2Cu_2Cl_2(\mu\text{-}Ph_2pz)_4(Ph_2pzH)_2]$ (**5**) also crystallizes with two acetonitrile molecules, and its crystal structure is isomorphous to that of **4**·2CH_3CN. The molecular structure of **5** is shown in Figure 6. Similarly to **4**, the complex molecule of **5** is formed by liberation of two protons in total

dx.doi.org/10.1021/ic202663q | Inorg. Chem. XXXX, XXX, XXX−XXX

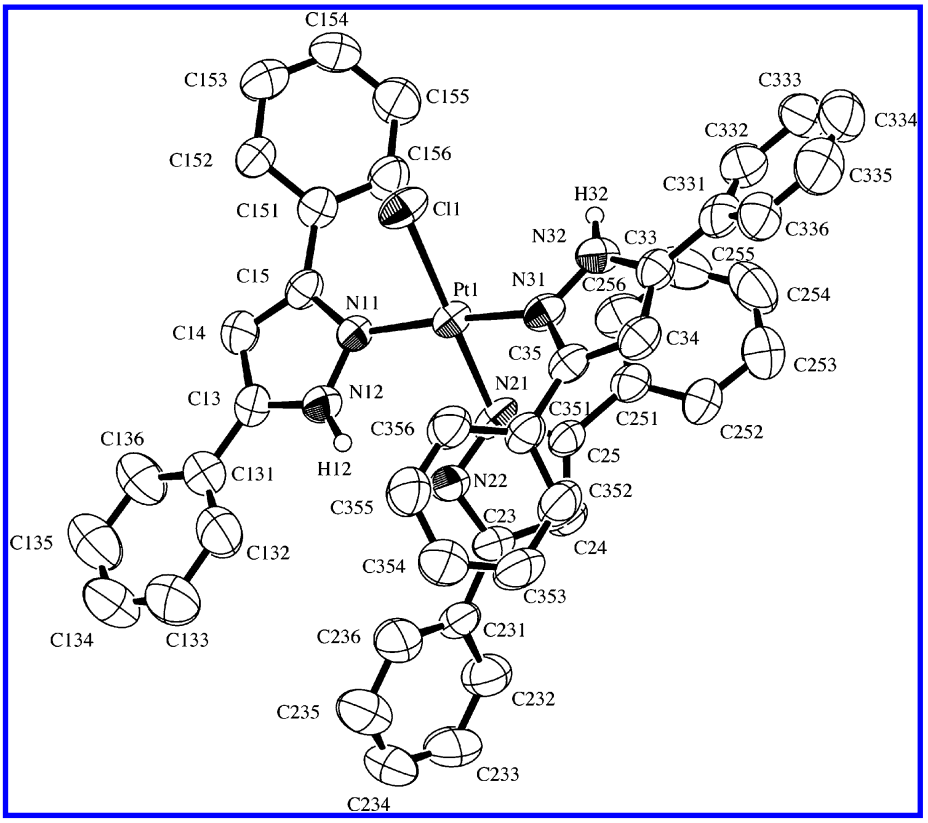

Figure 3. Molecular structure of **2** with the atom numbering scheme (50% probability ellipsoids).

from two molecules of **2** and incorporation of two Cu^{I} ions into the molecule. A chloride ion, two Ph_2pz anions and a neutral Ph_2pzH molecule coordinate to each Pt^{II} center, and each Cu^{I} ion is located between the two Ph_2pz ligands. The complex molecule also has a crystallographically imposed 2-fold axis passing through the midpoint of Pt1···Pt1* and the midpoint of Cu1···Cu1*, and half of the atoms in the molecule are independent. The Pt···Pt distance in **5** is 3.9614(3) Å, which is ca. 0.3 Å shorter than that in **4** due to the smaller ionic radius of Cu^{I} than that of Ag^{I} (Supporting Information Table S4). Nevertheless the Pt···Cu distances (3.3458(7) and 3.2127(7) Å) and the Cu···Cu distance (3.1465(10) Å) in **5** are not so much different from the Pt···Ag distances and Ag···Ag distance in **4**, respectively.

The monochloromono(dimethylpyrazolato) complex, $[Pt_2Ag_4(\mu\text{-}Cl)(\mu\text{-}Me_2pz)(Ph_2pz)_6]$ (**7**), crystallized in triclinic $P\bar{1}$. Because the asymmetric unit of **7** consists of two crystallographically independent molecules, one of them is illustrated in Figure 7. The complex **7** consists of two Pt atoms, four Ag atoms, a chloride ion, a Me_2pz anion, and six Ph_2pz anions. In a molecule, a chloride ion and three Ph_2pz anions coordinate to one of the two Pt atoms, and the other Pt atom is coordinated by a Me_2pz anion and three Ph_2pz anions. These two Pt units, $\{PtCl(Ph_2pz)_3\}$ and $\{Pt(Me_2pz)(Ph_2pz)_3\}$, sandwiches four Ag^{I} ions to form Pt_2Ag_4 distorted octahedron, each Ag^{I} ion being located between two Ph_2pz ligands, between chloride ligand and Ph_2pz ligand, and between Me_2pz ligand and Ph_2pz ligand. The overall structure of **7** is similar to that of dichloro complex **3**, though one of the chloride ligands is replaced by Me_2pz ligand. The Pt···Pt distances in **7** are 5.2345(7) and 5.1066(6) Å (Supporting Information Table S5), which are comparable to those in **3** (5.0276(8) Å) and $[Pt_2Ag_4(\mu\text{-}Me_2pz)_8]$ (5.1578(8) Å).[26] The large difference of Pt···Pt distances between two independent molecules in **7** may be attributed to a difference of packing effect. The Pt···Ag distances are ranging from 3.0925(11) to 3.5798(13) Å, and the proximate Ag···Ag distances are ranging from 2.9527(14) to 3.2964(15) Å. The Pt−Cl distances (2.329(4) and 2.346(4) Å) in **7** are comparable to those in **3** and **4**. The Ag−Cl distances (2.454(4) and 2.452(3) Å) and Pt−Cl−Ag angles (80.58(11) and 80.24(10)°) are also very similar to those in **3** (2.486(3) and 2.518(3) Å, and 80.82(8) and 76.43(6)°), respectively.

The molecular structure of bis(dimethylpyrazolato) complex $[Pt_2Ag_4(\mu\text{-}Me_2pz)_2(Ph_2pz)_6]$ (**8**) is shown in Figure 8. The complex **8** consists of two Pt atoms, four Ag atoms, two Me_2pz anions, and six Ph_2pz anions. Each Pt atom is coordinated by a Me_2pz anion and three Ph_2pz anions. Similarly to **3** and **7**, the two Pt units, $\{Pt(Me_2pz)(Ph_2pz)_3\}$, sandwiches four Ag^{I} ions to form Pt_2Ag_4 distorted octahedron, each Ag^{I} ion being located between two Ph_2pz ligands and between two Me_2pz ligands. It is noteworthy here that no Ag^{I} ion is located between Ph_2pz ligand and Me_2pz in this major isomer. Nevertheless the complex molecule also has an idealized 2-fold axis passing through Ag1 and Ag3. The Pt···Pt distance in **8** is 5.1001(9) Å (Supporting Information Table S6), which is comparable to those in **3** and **7**. The Pt···Ag distances are ranging from 3.3460(15) to 3.5822(14) Å, and the proximate Ag···Ag distances are ranging from 3.159(2) to 3.3514(18) Å. Those are also very similar to those in **3** and **7**.

Absorption and Emission Spectroscopy. The colorless mononuclear Pt^{II} complexes with Ph_2pz and/or Ph_2pzH ligands, **1**, **2**, and **6** exhibit absorption bands in the UV region shorter than 350 nm. On the contrary, the pale yellow heteropolynuclear complexes having chloride ligands exhibit weak absorption band tail in the range of 350−400 nm. The UV/vis absorption spectra of **2**, **3**, **6**, and **8** are shown in Figure

dx.doi.org/10.1021/ic202663q | Inorg. Chem. XXXX, XXX, XXX−XXX

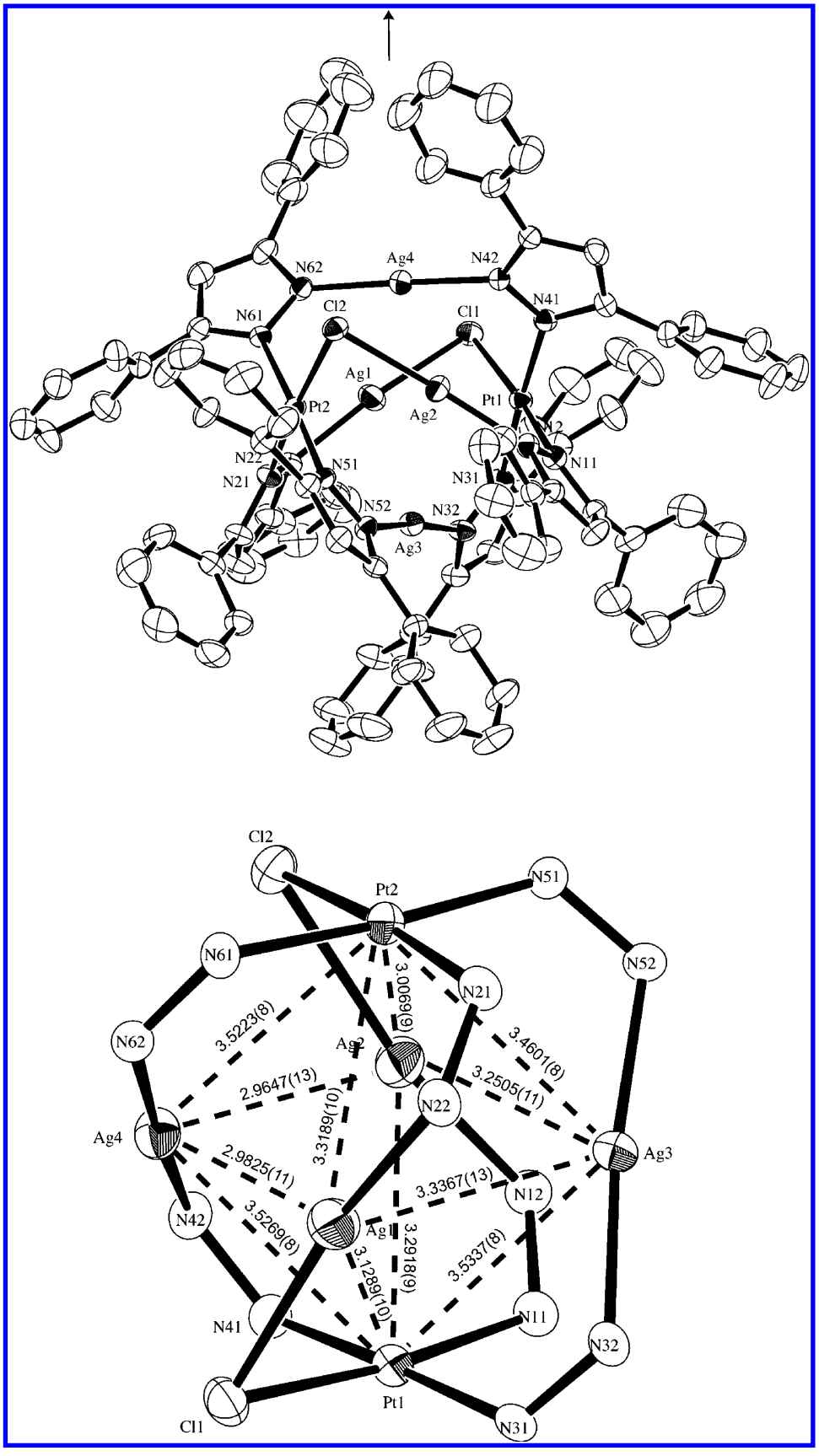

Figure 4. Molecular structure of **3** with the atom numbering scheme (30% probability ellipsoids) and metal−metal distances (Å) in **3**. The arrow indicates direction of idealized 2-fold axis.

dx.doi.org/10.1021/ic202663q | *Inorg. Chem.* XXXX, XXX, XXX−XXX

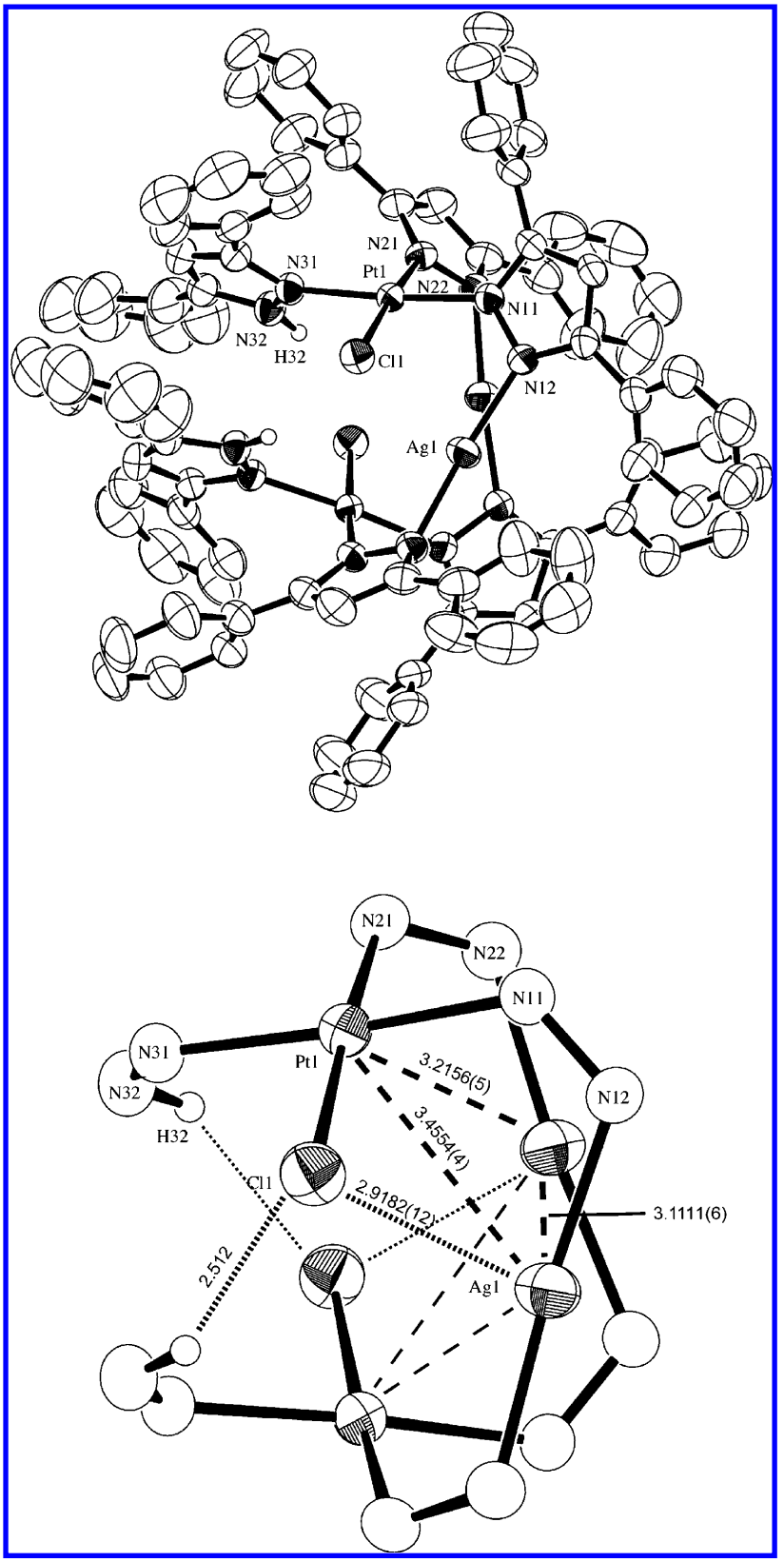

Figure 5. Molecular structure of **4** with the atom numbering scheme (50% probability ellipsoids) and metal–metal distances (Å) in **4**.

9; we omitted the spectra of **4** and **7** since the absorption spectra of heterohexanuclear Pt^{II} complexes **3**, **4**, and **7** resemble to each other (Supporting Information Figure S10). The photophysical data for **2**-**8** are summarized in Table 1. Both of these mononuclear Pt^{II} complexes and heteropolynuclear Pt^{II} complexes exhibit absorption bands arising from $\pi-\pi^*$ transition of Ph_2pz/Ph_2pzH at around 250 nm.

The mononuclear Pt^{II} complexes **1** and **2**, with a chloride ligand and Ph_2pzH or Ph_2pz do not exhibit emission in the solid state as well as in solution at an ambient temperature,

dx.doi.org/10.1021/ic202663q | *Inorg. Chem.* XXXX, XXX, XXX–XXX

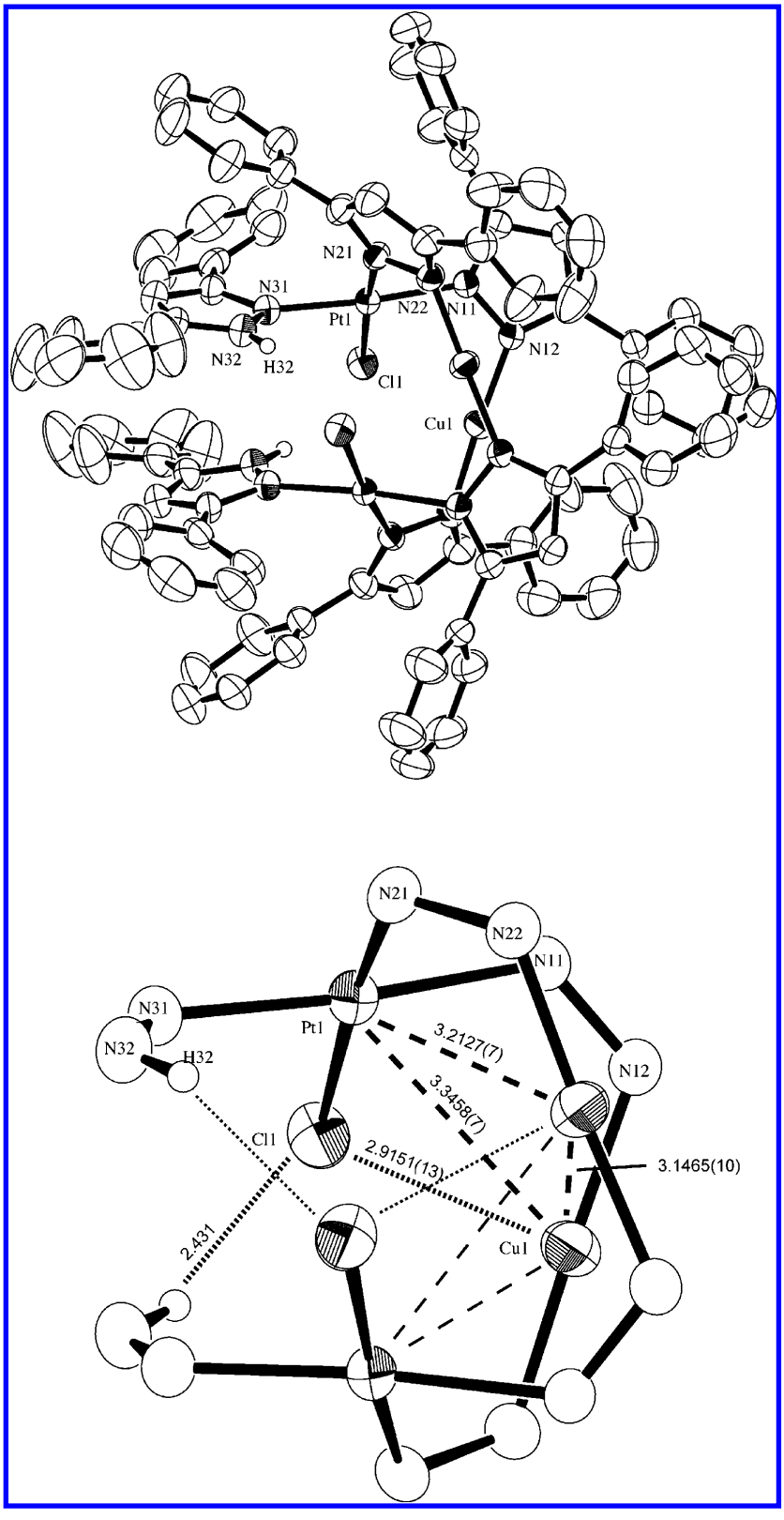

Figure 6. Molecular structure of **5** with the atom numbering scheme (50% probability ellipsoids) and metal–metal distances (Å) in **5**.

while the neutral chloride-free complex **6** exhibits weak green emission in the solid state (Supporting Information Figure S16). The reaction of **2** with Ag^{I} ion in a different Pt/Ag ratio afforded the $Pt_2Ag_4Cl_2$ complex **3** and the $Pt_2Ag_2Cl_2$ complex **4**, which exhibit red-orange emission (λ_{max} = 683 nm) and orange emission (λ_{max} = 626 nm), respectively, in the solid state at an ambient temperature (Figure 10). The $Pt_2Ag_4Cl(Me_2pz)$ complex **7**, obtained by two synthetic methods (Scheme 2), exhibits yellow-orange emission (λ_{max} = 599 nm) in the solid state (Figure 10). Although the dichloro complexes **3** and **4** also exhibit weak emission in CH_2Cl_2 solution at an ambient temperature, the emission spectra of these complexes are

dx.doi.org/10.1021/ic202663q | *Inorg. Chem.* XXXX, XXX, XXX–XXX

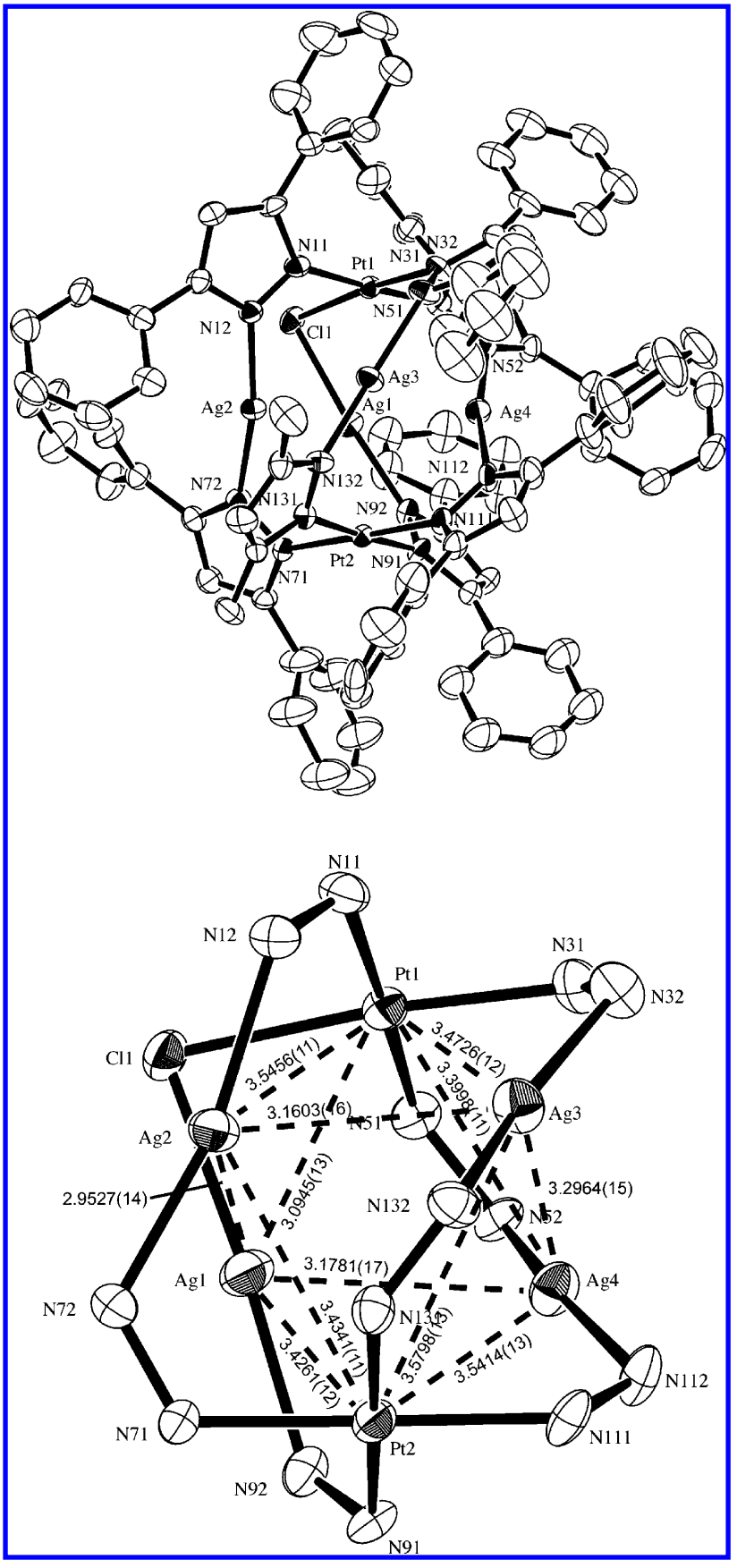

Figure 7. Molecular structure of 7 with the atom numbering scheme (30% probability ellipsoids) and metal−metal distances (Å) in 7.

dx.doi.org/10.1021/ic202663q | *Inorg. Chem.* XXXX, XXX, XXX−XXX

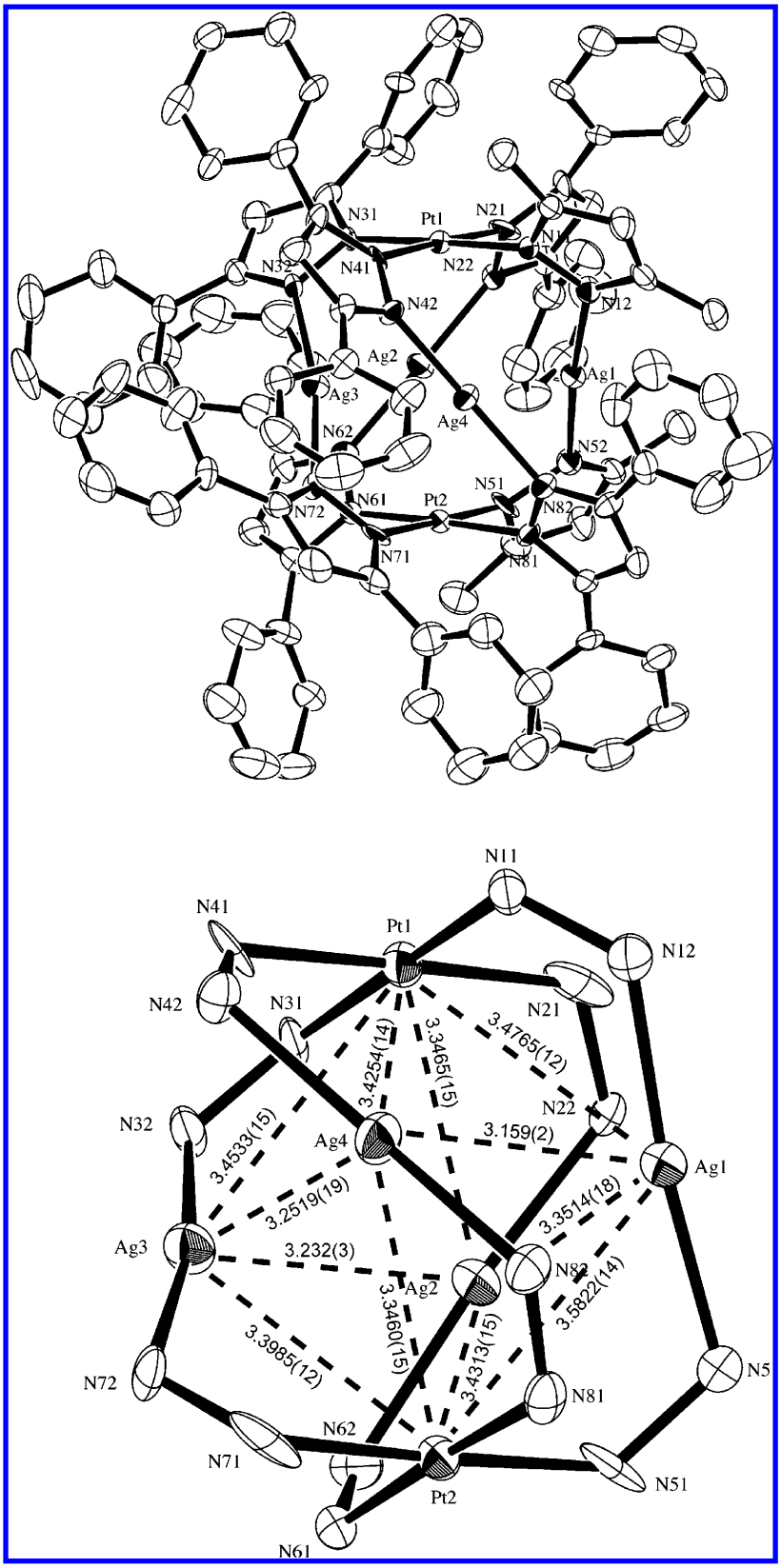

Figure 8. Molecular structure of **8** with the atom numbering scheme (30% probability ellipsoids) and metal–metal distances (Å) in **8**.

dependent on the excitation wavelength and slightly change with time. These characteristics are in contrast with those of Me_2pz-bridged Pt_2Ag_4 complex, $[Pt_2Ag_4(\mu\text{-}Me_2pz)_8]$,[26] the emission spectrum of which does not show the dependence on the excitation wavelength and does not change with time under irradiation of UV light in solution. The photophysical data for **3**, **4**, and **7** are listed in Table 1. The observed lifetimes of the emission for these complexes in the microsecond regime indicate that the emissions are phosphorescence. The solid state quantum yields of **3** (Φ_{em} = 0.07) and **7** (Φ_{em} = 0.16) are

dx.doi.org/10.1021/ic202663q | *Inorg. Chem.* XXXX, XXX, XXX–XXX

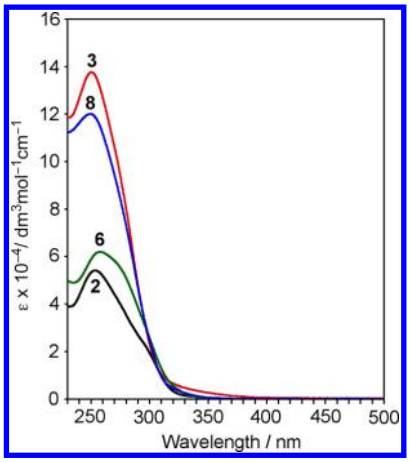

Figure 9. Electronic absorption spectra of **2** (black), **3** (red), **6** (green), and **8** (blue) in CH_2Cl_2 at 298 K.

Table 1. Photophysical Data for 2−8

complex	absorption[a] λ_{max} [nm] (ε_{max} [dm^3 mol^{-1}cm^{-1}])	emission[b] λ_{max} [nm] (τ [μs])	Φ_{em}[c]
2	253 (54300), 300 sh		
3	250 (138000), 290 sh, 330 sh	683 (τ_1 = 0.33 (A_1 = 0.73), τ_2 = 2.81 (A_2 = 0.27))[d]	0.07
4	253 (124000), 335 sh	626 (6.34)	0.41
5	255 (110000), 320 sh		
6	258 (64200), 285 sh	529	
7	251 (136000), 290 sh, 320 sh	599 (τ_1 = 1.41 (A_1 = 0.41), τ_2 = 9.00 (A_2 = 0.59))[d]	0.16
8	250 (121000), 290 sh, 320 sh	515 (τ_1 = 1.02 (A_1 = 0.92), τ_2 = 2.37 (A_2 = 0.08))[d] 522 (0.72)[a]	0.13

[a]In dichloromethane at 298 K. [b]In the solid state at 298 K. [c]Emission quantum yield in the solid state. [d]Emission decay curve was analyzed by the equation ($I(t) = A_1 \exp(-t/\tau_1) + A_2 \exp(-t/\tau_2)$) using the nonlinear least-squares method.

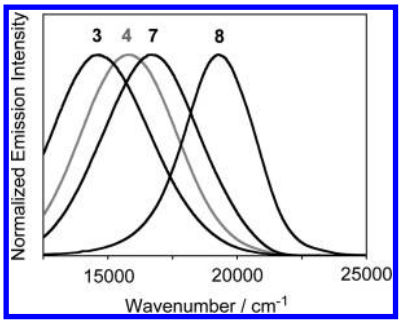

Figure 10. Normalized emission spectra of **3** (ν_{max} = 14600 cm^{-1} (683 nm)), **4** (ν_{max} = 16000 cm^{-1} (626 nm)), **7** (ν_{max} = 16700 cm^{-1} (599 nm)), and **8** (ν_{max} = 19200 cm^{-1} (515 nm)) in the solid state at 295 K (λ_{ex} = 355 nm).

moderate, while that of **4** (Φ_{em} = 0.41) is found to be very high at an ambient temperature. However, the emission of $Pt_2Cu_2Cl_2$ complex **5** was not observed in the range of 300−950 nm. Because the LUMO of **5**, similarly to **4**, mainly consists of π^* orbitals of monodentate Ph_2pzH ligands and the energy level of HOMO of **5** (Cu(d)) is higher than that of **4** (Pt(5d)), it is expected that the emission energy of **5** is lower than that of **4** (vide infra). The reason why the emission of **5** was not observed is unclear at this stage.

The chloride-free Pt_2Ag_4 complex bridged by Ph_2pz and Me_2pz, **8**, was found to exhibit green emission (λ_{max} = 515 nm) in the solid state at an ambient temperature (Figure 10). The solid-state quantum yield of **8** (Φ_{em} = 0.16) was moderate (Table 1). It should be emphasized that these photophysical data provided the answer for our original question why Pt_2Ag_4 complexes of 3,5-diphenylpyrazolate having chloride ligands exhibit orange to red-orange emission in spite of the sky-blue to green emission of the Pt_2Ag_4 complexes with 3,5-dialkylpyrazolates (R_2pz), $[Pt_2Ag_4(\mu\text{-}R_2pz)_8]$.[26] Now it is obvious that the low energy shift of the emission spectra was induced by the coordination of chloride ligands to the Pt^{II} centers. Very interestingly, systematic red shift of the emission energies with increase of chloride/pyrazolate ratio was observed for **3**, **7**, and **8** (Figure 10). It indicates that the coordination of a chloride ligand to one of the two Pt^{II} centers affects the whole orbital energies of **7**. The HOMOs as well as HOMO-1s of **3**, **7**, and **8** mainly consist of dδ orbitals of Pt^{II} centers and π orbitals of Ph_2pz ligands (vide infra). The LUMO of **8** mainly consists of in-phase combination of 6p of two Pt^{II} centers and 5p of four Ag^{I} centers, and those of **3** and **7** also mainly consist of similar pσ orbitals stabilized by the coordination of chlorido ligands to Pt^{II} centers. Therefore, it is likely that the emissions of **3**, **7**, and **8** are attributed to emissive states derived from the $Pt_2(d)/\pi \rightarrow Pt_2Ag_4$ transitions, the emission energy of which depends on the ratio of chloride ligands to pyrazolate ligands.

Although the shift of emission energies has been reported by the replacement of a chloride ligand in the Pt^{II} complex with an iodide ion,[32] the stepwise replacement of chloride ligands in the complex molecule with other ligands has not been studied probably due to the difficulty in the control of substitution reaction for the mononuclear Pt^{II} complex. The heterohexanuclear Pt^{II} complexes, **3**, **7**, and **8**, demonstrated for the first time that the emission energies of the Pt_2Ag_4 complexes could be shifted systematically by changing the ratio of coordinated chloride ligands to pyrazolate ligands.

Computational Study. To provide better understanding of the origin of the low-energy absorption bands of the heterohexanuclear Pt^{II} complexes, DFT calculations were performed on the ground states of **3**−**5**, **7**, and **8**. The selected molecular orbitals near frontier orbitals are depicted in Figure 11. The highest occupied molecular orbitals (HOMOs) as well as HOMO-1s of the heterohexanuclear complexes, **3**, **7**, and **8**, having Pt_2Ag_4 core, mainly consist of dδ orbital of Pt^{II} and π orbitals of Ph_2pz ligands. Their lowest unoccupied molecular orbitals (LUMOs) mainly consist of in-phase combination of 6p of two Pt^{II} centers and 5p of four Ag^{I} centers. The LUMOs of **3**, **7**, and **8** resemble well those of $[Pt_2M_4(\mu\text{-}Me_2pz)_8]$ (M = Ag, Cu)[26] and $[Pt_2Au_2M_2(\mu\text{-}Me_2pz)_8]$ (M = Ag, Cu),[27] and the absorption bands of $[Pt_2M_4(\mu\text{-}Me_2pz)_8]$ and $[Pt_2Au_2M_2(\mu\text{-}Me_2pz)_8]$ are assigned to $[Pt_2 \rightarrow Pt_2M_4]$ and $[Pt_2 \rightarrow Pt_2Au_2M_2]$ transitions, respectively. Theoretical calculations by the time-dependent density functional theory (TD-DFT) for **3**, **7**, and **8** revealed that the excitations with large oscillator strength were assigned to be $\pi \rightarrow \pi^*$ excitation in Ph_2pz ligands but the lowest excited state, which is assigned to be HOMO and/or HOMO-1 to LUMO excitation, exhibits small oscillator strength; see Supporting Information Figures S19−S24. The lowest energy absorption bands are assigned to $[Pt_2(d)/\pi \rightarrow Pt_2Ag_4]$ transition for **3**, **7**, and **8**. Careful examination of the DFT computational results further revealed that the 3p orbitals of Cl atoms interact with 6p orbitals of Pt^{II} centers and 5p orbitals of Ag^{I} centers in the same phase. It is obviously shown

dx.doi.org/10.1021/ic202663q | Inorg. Chem. XXXX, XXX, XXX−XXX

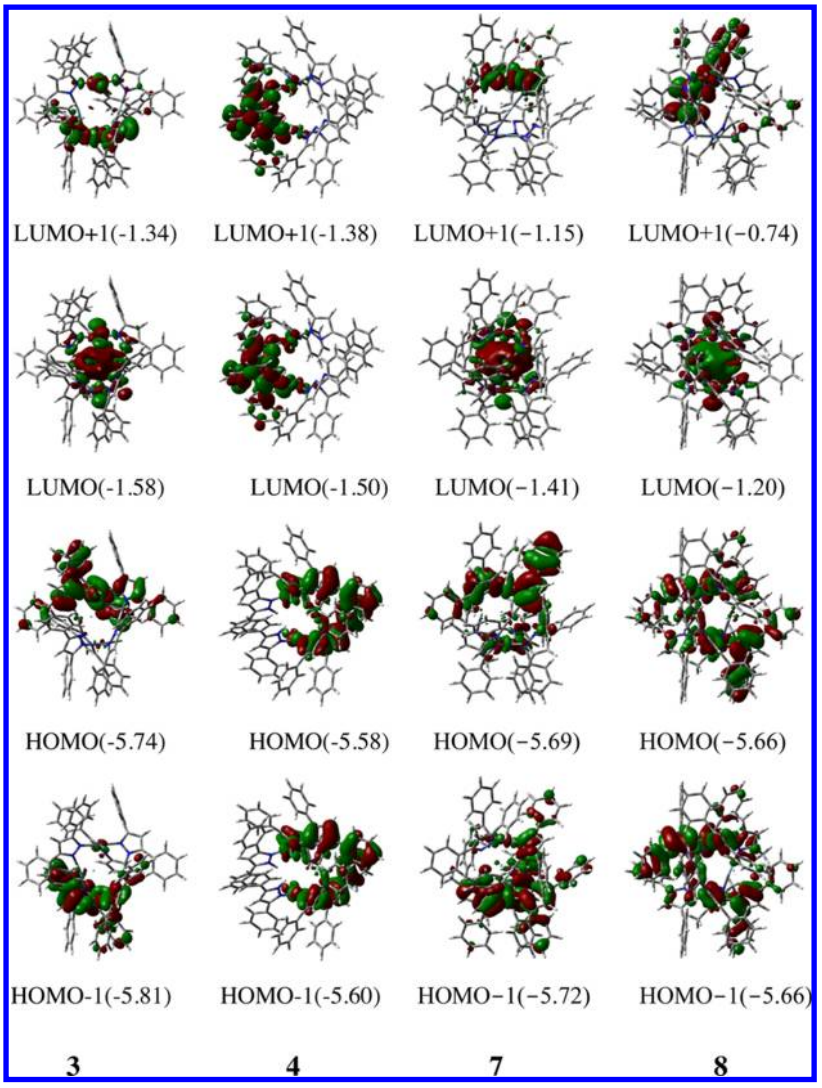

Figure 11. Spatial plot (isovalue = 0.02) of selected molecular orbitals of the singlet state for **3**, **4**, **7**, and **8** by the B3LYP method.

Table 2. Orbital Composition Percentages of Selected Molecular Orbitals for 3, 4, 7, and 8[a]

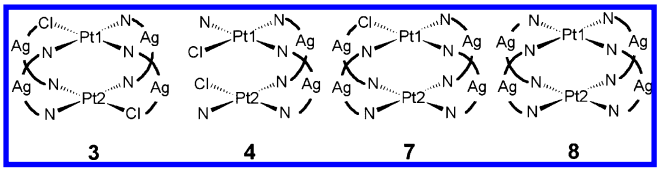

		HOMO−1				HOMO				LUMO				LUMO+1			
		3	**4**	**7**	**8**	**3**	**4**	**7**	**8**	**3**	**4**	**7**	**8**	**3**	**4**	**7**	**8**
Pt	(Pt1)	14	7	2	6	0	6	10	8	6	2	6	6	33	1	44	0
	(Pt2)	1	7	12	10	13	6	3	6	6	2	5	6	7	1	0	3
Ag		1	1	1	0	1	2	1	1	55	0	52	49	5	0	4	2
Cl		1	3	0		1	2	1		6	1	3		11	1	13	
Other		83	82	85	84	85	84	85	85	27	95	34	39	44	97	39	95

[a]The composition percentages were expressed in terms of contributions from each Pt metal center, four or two Ag metal centers, Cl ligands, and Ph_2pz ligands (including neutral Ph_2pzH ligands for **4**).

that the contribution of Cl atoms to LUMO (6% for **3** ($Pt_2Ag_4Cl_2$) and 3% for **7** (Pt_2Ag_4Cl)) increases with increase of chloride/pyrazolate ratio, while the Cl atom little contributes to the HOMO (less than 1%) (Table 2). Though the calculated HOMO−LUMO energy difference is not exactly the same as the emission energy, in particular, in the case of the phosphorescence, the decreasing trend of the LUMO energy is parallel to the decreasing order of the emission energy (Figure 11). This suggests that the trend of emission energy is mainly determined by the LUMO energy shift. Therefore the coordination of chloride ligands to Pt^{II} centers stabilizes the

dx.doi.org/10.1021/ic202663q | *Inorg. Chem.* XXXX, XXX, XXX−XXX

LUMOs of **3** and **7**, leading to the red shift of the emission spectra.

In contrast, the HOMO of **4** mainly consists of dδ orbital of Pt^{II} mixing with π^* orbitals of bridging Ph_2pz ligands, and the LUMO of **4** mainly consists of π^* orbitals of neutral Ph_2pzH ligands which are monodentate ligands. Thus it is likely that the low-energy absorption bands of **4** include the ligand-to-ligand charge-transfer (LLCT) and the metal-to-ligand charge-transfer (MLCT) transitions. Similarly to $[Pt_2Cu_4(\mu\text{-}Me_2pz)_8]$[26] and $[Pt_2Au_2Cu_2(\mu\text{-}Me_2pz)_8]$,[27] the HOMO of **5** also mainly consists of Cu d orbitals, owing to higher orbital energy of Cu(3d) than that of Pt(5d). Since the LUMO of **5** mainly consists of π^* orbitals of neutral monodentate Ph_2pzH ligands, the low-energy absorption bands of **5** contain the MLCT character (Supporting Information Table S11).

CONCLUSIONS

By taking advantages of weak basicity and bulkiness of 3,5-diphenylpyrazole, we succeeded to prepare the mononuclear Pt^{II} complex consisting of three neutral Ph_2pzH ligands and a chloride ligand, **1**. The treatment of **1** with a base and successive reaction with Ag^I give the $Pt_2Ag_4Cl_2$ complex, **3**, which exhibits red-orange emission in the solid state at an ambient temperature. The red-orange emission of **3** is very unique, because the Pt_2Ag_4 complexes with 3,5-dialkylpyrazolate, $[Pt_2Ag_4(\mu\text{-}R_2pz)_8]$, has tendency to exhibit sky-blue to green emission. The replacement of chloride ligands in **3** with Me_2pz ligands afforded the $Pt_2Ag_4Cl(Me_2pz)$ complex, **7**, and the $Pt_2Ag_4(Me_2pz)_2$ complex, **8**, respectively. The red-orange emission of **3**, yellow-orange emission of **7**, and green emission of **8** revealed that the emission energies of the series of heterohexanuclear Pt^{II} complexes is systematically modulated by the ratio of coordinated chloride ligands to pyrazolate ligands. It implies that the coordination of chloride ligands to Pt^{II} ions affects the whole orbital energies of Pt_2Ag_4 complexes. DFT calculations indicate that the highest occupied molecular orbital (HOMO) as well as HOMO-1 of the heterohexanuclear complexes, **3**, **7**, and **8**, having Pt_2Ag_4 core, mainly consists of dδ orbital of Pt^{II} and π orbitals of Ph_2pz ligands, while the lowest unoccupied molecular orbital (LUMO) of these complexes mainly consists of in-phase combination of 6p of two Pt^{II} centers and 5p of four Ag^I centers. Thus it is likely that the emissions of **3**, **7**, and **8** are attributed to emissive states derived from the $Pt_2(d)/\pi \rightarrow Pt_2Ag_4$ transitions. Careful examination of the DFT computational results further revealed that the bonding contribution of Cl atoms to LUMO increases with increase of chloride/pyrazolate ratio, while the Cl atom little contributes to the HOMO. These results are consistent with the fact that the coordination of chloride ligands to Pt^{II} centers stabilizes the LUMOs of **3** and **7**, leading to the red shift of the emission spectrum.

EXPERIMENTAL SECTION

Materials. $[PtCl_2(C_2H_5CN)_2]$ was prepared by the literature methods.[33] All other commercially available reagents were used as purchased.

Physical Measurement and Instrumentation. UV−vis and diffuse reflectance spectra were recorded on a Hitachi U-3300 spectrophotometer and a Jasco V-560 spectrophotometer at 20 °C. Electrical conductivity was measured using a TOA EC meter CM-30G. The ^{1}H NMR spectra were obtained at 300 MHz with a Varian Gemini 300 spectrometer. The variable-temperature ^{1}H NMR spectra were obtained at 400 MHz with a JEOL JNM-AL400 spectrometer. Corrected emission spectra were obtained by using a red-sensitive photodetector (Hamamatsu PMA-11, model C5966−23) and the third-harmonic generation of an Nd:YAG Laser (Continuum Surelite) at 355 nm excitation. The instrumental responses of the system were corrected by using a software package for the detector. Lifetime measurements were conducted by using a streak camera (Hamamatsu C4334) as a detector. Emission quantum yields in the solid state were determined by using a Hamamatsu Photonic Absolute PL Quantum Yield Measurement System C9920−02. Powder X-ray diffraction patterns were measured on a Rigaku RINT-2200VL diffractometer using graphite-monochromated Cu Kα (λ = 1.5418 Å) radiation at 296 K.

Preparation of Complexes. *$[PtCl(Ph_2pzH)_3]Cl$ (**1**).* A toluene solution (15 mL) of Ph_2pzH (136 mg, 0.62 mmol) was added to a suspension of $[PtCl_2(C_2H_5CN)_2]$ (60 mg, 0.16 mmol) in toluene (5 mL), and the suspension was refluxed for 10 h under an argon atmosphere. Yellowish-white precipitate was filtered, washed with toluene, hexane and diethyl ether, and dried in vacuo. Yield: 137 mg (93%). Anal. Calcd for $C_{45}H_{36}Cl_2N_6Pt$: C, 58.32; H, 3.92; N, 9.07. Found: C, 58.38; H, 3.92; N, 9.11. ^{1}H NMR (300 MHz, $CDCl_3$, 25 °C, TMS): δ = 15.52 (s, 1H, NH), 14.40 (s, 2H, NH), 8.22−8.19 (m, 4H, Ph), 7.92 (d, J = 7.2 Hz, 4H, Ph), 7.83 (d, J = 7.1 Hz, 2H, Ph), 7.52−7.34 (m, 15H, Ph), 7.09 (d, J = 7.0 Hz, 2H, Ph), 6.91 (d, J = 7.3 Hz, 1H, Ph), 6.65 (d, J = 2.1 Hz, 2H, H_4), 6.59 (t, J = 7.6 Hz, 2H, Ph), 6.39 ppm (d, J = 2.3 Hz, 1H, H_4). FABMS: m/z 891.3 $[M - Cl]^+$.

*$[PtCl(Ph_2pz)(Ph_2pzH)_2]$ (**2**).* A solution of KOH (35 mg, 0.62 mmol) in methanol (2 mL) was added dropwise to a suspension of **1** (198 mg, 0.21 mmol) in methanol (18 mL) with stirring at 25 °C, so that the white-yellow suspension immediately changed to white. After stirring for 1 h, the formed white solid was collected, washed with methanol and water, and then dried in vacuo. Yield: 173 mg (91%). Anal. Calcd for $C_{45}H_{35}ClN_6Pt$: C, 60.71; H, 3.96; N, 9.44. Found: C, 60.68; H, 3.93; N, 9.29. ^{1}H NMR (300 MHz, $CDCl_3$, 25 °C, TMS): δ = 8.12 (d, J = 7.7 Hz, 4H, Ph of Ph_2pzH), 7.93 (d, J = 7.7 Hz, 2H, Ph of Ph_2pz), 7.50−7.23 (m, 21H, Ph), 7.25 (t, J = 7.6 Hz, 2H, Ph of Ph_2pz), 7.06 (t, J = 7.4 Hz, 1H, Ph of Ph_2pz), 6.45 (s, 2H, H_4 of Ph_2pzH), 6.24 ppm (s, 1H, H_4 of Ph_2pz). FABMS: m/z 890.3 $[M]^+$.

*$[Pt_2Ag_4(\mu\text{-}Cl)_2(\mu\text{-}Ph_2pz)_6]$ (**3**).* To a suspension of **2** (54 mg, 0.061 mmol) in acetonitrile (10 mL) were added Et_3N (18 mg, 0.18 mmol) and a solution of $AgBF_4$ (26 mg, 0.13 mmol) in acetonitrile (10 mL). The suspension was stirred for 5 h at 25 °C to give a clear solution. After filtration, the filtrate was concentrated almost to dryness by a rotary evaporator. Methanol (30 mL) was added to the flask. The resulted white precipitate was collected, washed with methanol, and then dried in vacuo. Yield: 59 mg (89%). It was recrystallized from CH_2Cl_2/CH_3OH. Anal. Calcd for $C_{90}H_{66}Ag_4Cl_2N_{12}Pt_2$: C, 48.96; H, 3.01; N, 7.61. Found: C, 48.89; H, 2.90; N, 7.64. ^{1}H NMR (300 MHz, $CDCl_3$, 25 °C, TMS): δ = 7.78 (d, J = 7.1 Hz, 4H, Ph), 7.68−7.65 (m, 4H, Ph), 7.47−7.36 (m, 14H, Ph), 7.24−7.16 (m, 10H, Ph), 7.09−7.03 (m, 8H, Ph), 6.87 (d, J = 4.4 Hz, 10H, Ph), 6.83 (s, 2H, Ph), 6.70 (t, J = 7.5 Hz, 4H, Ph), 6.36 (d, J = 2.4 Hz, 2H, H_4), 5.97 (d, J = 2.6 Hz, 2H, H_4), 5.88 (d, J = 2.5 Hz, 2H, H_4), 5.85 (d, J = 6.9 Hz, 4H, Ph). FABMS: m/z 2208.1 $[M + H]^+$

*$[Pt_2Ag_2Cl_2(\mu\text{-}Ph_2pz)_4(Ph_2pzH)_2]$ (**4**). Method A.* To a suspension of **2** (58 mg, 0.065 mmol) in acetonitrile (8 mL) was added a solution of $AgBF_4$ (26 mg, 0.13 mmol) in acetonitrile (10 mL). The suspension was stirred for 2 h at 25 °C, and the resulted white precipitate was collected, washed with acetonitrile, and dried in vacuo. Yield: 27 mg (45%). It was recrystallized from $CHCl_3/CH_3CN$. Anal. Calcd for $C_{90}H_{68}Ag_2Cl_2N_{12}Pt_2$: C, 54.20; H, 3.44; N, 8.43. Found: C, 53.84; H, 3.39; N, 8.46. ^{1}H NMR (300 MHz, $CDCl_3$, 25 °C, TMS): δ = 11.34 (s, 2H, NH), 7.98 (d, J = 7.0 Hz, 2H, Ph), 7.90−7.87 (m, 4H, Ph), 7.73 (d, J = 7.3 Hz, 4H, Ph), 7.67 (d, J = 6.9 Hz, 4H, Ph), 7.48 (d, J = 6.5 Hz, 4H, Ph), 7.43−7.06 (m, 26H, Ph), 6.97 (t, J = 7.4 Hz, 2H, Ph), 6.86−6.69 (m, 4H, Ph), 6.61 (d, J = 2.2 Hz, 2H, H_4), 6.52 (t, J = 7.4 Hz, 2H, Ph), 6.32 (t, J = 7.5 Hz, 4H, Ph), 6.15 (d, J = 2.0 Hz, 2H, H_4), 5.93 (d, J = 6.9 Hz, 4H, Ph), 5.68 ppm (s, 2H, H_4).

Method B. To a suspension of **2** (60 mg, 0.067 mmol) in acetonitrile (8 mL) were added Et_3N (6.1 mg, 0.060 mmol) and a solution of $AgBF_4$ (13 mg, 0.065 mmol) in acetonitrile (10 mL). The suspension was stirred for 6 h at 25 °C, and the resulted white

dx.doi.org/10.1021/ic202663q | Inorg. Chem. XXXX, XXX, XXX−XXX

Table 3. Crystallographic Data for $[PtCl(Ph_2pz)(Ph_2pzH)_2]\cdot CH_3OH$ ($2\cdot CH_3OH$), $[Pt_2Ag_4(\mu\text{-}Cl)_2(\mu\text{-}Ph_2pz)_6]\cdot 3CH_2Cl_2$ ($3\cdot 3CH_2Cl_2$), $[Pt_2Ag_2Cl_2(\mu\text{-}Ph_2pz)_4(Ph_2pzH)_2]\cdot 2CH_3CN$ ($4\cdot 2CH_3CN$), $[Pt_2Cu_2Cl_2(\mu\text{-}Ph_2pz)_4(Ph_2pzH)_2]\cdot 2CH_3CN$ ($5\cdot 2CH_3CN$), $[Pt_2Ag_4(\mu\text{-}Cl)(\mu\text{-}Me_2pz)(\mu\text{-}Ph_2pz)_6]\cdot 0.5CH_3OH\cdot 0.5H_2O$ ($7\cdot 0.5CH_3OH\cdot 0.5H_2O$), and $[Pt_2Ag_4(\mu\text{-}Me_2pz)_2(\mu\text{-}Ph_2pz)_6]$ (8)

	$2\cdot CH_3OH$	$3\cdot 3CH_2Cl_2$	$4\cdot 2CH_3CN$
formula	$C_{46}H_{39}ClN_6OPt$	$C_{93}H_{72}Ag_4Cl_8N_{12}Pt_2$	$C_{94}H_{74}Ag_2Cl_2N_{14}Pt_2$
fw	922.40	2462.95	2076.53
T [K]	296	296	296
λ [Å]	0.71070	0.71070	0.71070
crystal systems	monoclinic	triclinic	orthorhombic
space group	$P2_1/n$ (14)	$P\bar{1}$ (2)	$Pnna$ (52)
a [Å]	15.8874(10)	15.438(3)	18.1830(4)
b [Å]	9.6977(4)	17.477(3)	22.6303(5)
c [Å]	27.367(2)	17.818(3)	20.1687(4)
α [deg]	90	80.488(3)	90
β [deg]	105.6240(9)	84.636(3)	90
γ [deg]	90	77.718(3)	90
V [Å^3]	4060.7(4)	4624.3(12)	8299.1(3)
Z	4	2	4
ρ_{calcd} [g cm^{-3}]	1.509	1.769	1.662
μ(Mo Kα) [mm^{-1}]	3.550	4.112	3.931
reflns collected	29287	35378	59486
no. unique reflns	9132 (R_{int} = 0.0493)	19799 (R_{int} = 0.025)	9437 (R_{int} = 0.028)
final R indices[a]	R_1 = 0.072 [$I > 2\sigma(I)$]	R_1 = 0.060 [$I > 2\sigma(I)$]	R_1 = 0.042 [$I > 2\sigma(I)$]
R indices[b,c]	R = 0.090,[d] R_w = 0.115[d]	R = 0.069,[d] R_w = 0.174[d]	R = 0.046,[d] R_w = 0.086[d]
goodness-of-fit on F^2	1.290	1.10	1.22
	$5\cdot 2CH_3CN$	$7\cdot 0.5CH_3OH\cdot 0.5H_2O$	8
formula	$C_{94}H_{74}Cl_2Cu_2N_{14}Pt_2$	$C_{95.5}H_{76}Ag_4ClN_{14}Pt_2$	$C_{100}H_{80}Ag_4N_{16}Pt_2$
fw	1987.89	2292.85	2327.49
T [K]	296	296	296
λ [Å]	0.71070	0.71070	0.71070
crystal systems	orthorhombic	triclinic	triclinic
space group	$Pnna$ (52)	$P\bar{1}$ (2)	$P\bar{1}$ (2)
a [Å]	18.3146(5)	13.8447(4)	14.544(2)
b [Å]	22.6251(5)	15.3018(5)	14.751(2)
c [Å]	19.7815(5)	41.1566(13)	22.063(2)
α [deg]	90	94.524(2)	95.221(3)
β [deg]	90	92.992(2)	92.255(3)
γ [deg]	90	90.787(2)	112.527(4)
V [Å^3]	8196.9(4)	8678.6(5)	4339.9(7)
Z	4	4	2
ρ_{calcd} [g cm^{-3}]	1.611	1.755	1.781
μ(Mo Kα) [mm^{-1}]	4.023	4.168	4.139
rflns collected	58362	54612	32572
no. of unique rflns	9141 (R_{int} = 0.029)	32082 (R_{int} = 0.038)	18453 (R_{int} = 0.061)
final R indices[a]	R_1 = 0.045 [$I > 2\sigma(I)$]	R_1 = 0.071 [$I > 2\sigma(I)$]	R_1 = 0.097 [$I > 2\sigma(I)$]
R indices[b,c]	R = 0.047,[d] R_w = 0.091[d]	R = 0.078, R_w = 0.212	R = 0.110, R_w = 0.302
goodness-of-fit on F^2	1.21	1.13	1.08

[a] $R_1 = \sum||F_o| - |F_c||/\Sigma|F_o|$. [b] $R = \sum(F_o^2 - F_c^2)/\sum F_o^2$. [c] $R_w = [\sum[w(F_o^2 - F_c^2)^2]/\sum[w(F_o^2)^2]]^{1/2}$. [d] All data.

precipitate was collected, washed with acetonitrile, and dried in vacuo. Yield: 60 mg (89%). It was recrystallized from $CHCl_3/CH_3CN$.

*$[Pt_2Cu_2Cl_2(\mu\text{-}Ph_2pz)_4(Ph_2pzH)_2]$ (**5**).* To a solution of **2** (149 mg, 0.17 mmol) in dichloromethane (7 mL) were added a solution of $[Cu(CH_3CN)_4]BF_4$ (61 mg, 0.19 mmol) in dichloromethane (10 mL) and Et_3N (18 mg, 0.18 mmol). The solution turned to yellow suspension immediately after the addition of Et_3N, and the suspension was stirred for 6 h to give pale yellow solution. The solution was evaporated to dryness. The resulted solid was collected, washed with acetonitrile and diethyl ether, and dried in vacuo. Yield: 128 mg (80%). It was recrystallized from $CHCl_3/CH_3CN$. Anal. Calcd for $C_{90}H_{68}Cu_2Cl_2N_{12}Pt_2$: C, 56.72; H, 3.60; N, 8.82. Found: C, 56.43; H, 3.41; N, 8.86. ^{1}H NMR (300 MHz, $CDCl_3$, 25 °C, TMS): δ = 11.53 (d, J = 1.7 Hz, 2H, NH), 7.66–7.58 (m, 12H, Ph), 7.47 (d, J = 1.5 Hz, 2H, Ph), 7.45 (s, 2H, Ph), 7.36 (t, J = 7.4 Hz, 4H, Ph), 7.31–7.04 (m, 18H, Ph), 6.95–6.90 (m, 8H, Ph), 6.77 (t, J = 7.6 Hz, 4H, Ph), 6.56 (s, 2H, H_4), 6.51 (d, J = 7.5 Hz, 2H, Ph), 6.40 (t, J = 7.5 Hz, 4H, Ph), 6.10 (s, 2H, H_4), 5.94 (d, J = 7.7 Hz, 4H, Ph), 5.72 ppm (d, J = 2.2 Hz, 2H, H_4).

*$[Pt(Ph_2pz)_2(Me_2pzH)(Ph_2pzH)]$ (**6**).* A solution of KOH (40 mg, 0.71 mmol) in methanol (5 mL) was added to a solution of Me_2pzH (68 mg, 0.71 mmol) in methanol (5 mL), and the mixture was stirred for 10 min at 25 °C. A solid of $K[Me_2pz]$ was obtained by removing solvent from the solution. To a flask containing $K[Me_2pz]$ was added a solution of **2** (577 mg, 0.65 mmol) in acetonitrile (40 mL), and the solution was refluxed for 24 h under an argon atmosphere. Reduction

dx.doi.org/10.1021/ic202663q | Inorg. Chem. XXXX, XXX, XXX–XXX

of the solution volume gave white precipitate. It was collected, washed with acetonitrile and hexane, and dried in vacuo. Yield: 248 mg (40%). Recrystallization from $CHCl_3/CH_3OH$ gave fine crystals, which include chloroform molecules as solvent of crystallization. Anal. Calcd for $C_{51}H_{43}Cl_3N_8Pt$ (**6**·$CHCl_3$): C, 57.28; H, 4.05; N, 10.48. Found: C, 57.28; H, 3.90; N, 10.48. ^{1}H NMR (400 MHz, $CDCl_3$, −50 °C, TMS): δ = 7.97 (m, 7H, Ph), 7.84 (d, J = 7.4 Hz, 2H, Ph), 7.51−7.24 (m, 19H, Ph), 7.06 (m, 2H, Ph), 6.70 (s, 1H, H_4 of Ph_2pz), 6.21 (s, 1H, H_4 of Ph_2pz), 6.04 (s, 1H, H_4 of Ph_2pz), 5.48 (s, 1H, H_4 of Me_2pz), 1.97 (s, 3H, Me), 1.71 ppm (s, 3H, Me). FABMS: m/z 950.4 $[M + H]^+$.

*[Pt_2Ag_4(μ-Cl)(μ-Me_2pz)(μ-Ph_2pz)$_6$] (**7**). Method A.* To a suspension of **1** (301 mg, 0.33 mmol) were added a solution of Me_2pzH (34 mg, 0.35 mmol) in acetonitrile (10 mL) and Et_3N (32 mg, 0.32 mmol). The suspension was refluxed for 5 h under an argon atmosphere. The formed yellow-white solid was collected, washed with hexane and methanol, and dried in vacuo. Yield: 180 mg. ^{1}H NMR spectrum, FABMS (m/z 890.3, 950.4), and the molar conductivity indicate that the solid consists of **2** and **6** (see Supporting Information). This solid was used for further reaction with silver ion without purification. To a suspension of the above solid (107 mg) in acetonitrile (30 mL) were added a solution of $AgBF_4$ (82 mg, 0.42 mmol) in acetonitrile (10 mL) and Et_3N (22 mg, 0.22 mmol). The suspension was stirred for 3 h at 25 °C. Reduction of the solution volume gave white precipitate. It was collected, washed with methanol, and dried in vacuo. The precipitate was dissolved into chloroform to separate the fine solid of AgCl from the solution. An addition of methanol to the solution followed by slow evaporation of the solution gave crystalline compound. Yield: 41 mg (19% (based on **1**)). Anal. Calcd for $C_{95}H_{73}Ag_4ClN_{14}Pt_2$: C, 50.32; H, 3.24; N, 8.65. Found: C, 50.16; H, 3.04; N, 8.33. ^{1}H NMR (300 MHz, $CDCl_3$, 25 °C, TMS): δ = 7.82 (d, J = 6.9 Hz, 2H, Ph), 7.48−6.77 (m, 52H, Ph), 6.67 (t, J = 7.3 Hz, 2H, Ph), 6.40 (d, J = 2.5 Hz, 1H, H_4 of Ph_2pz), 6.33 (d, J = 2.5 Hz, 1H, H_4 of Ph_2pz), 6.18 (d, J = 6.9 Hz, 2H, Ph),6.11 (d, J = 2.7 Hz, 1H, H_4 of Ph_2pz), 5.92 (d, J = 6.9 Hz, 2H, Ph), 5.88 (d, J = 2.5 Hz, 2H, H_4 of Ph_2pz), 5.78 (d, J = 2.7 Hz, 1H, H_4 of Ph_2pz), 5.11 (d, J = 2.3 Hz, 1H, H_4 of Me_2pz), 1.56 (s, 3H, Me), 1.24 ppm (s, 3H, Me). FABMS: m/z 2268.1 $[M]^+$.

Method B. To a solution containing **2** (45 mg, 0.051 mmol) and **6** (48 mg, 0.050 mmol) in acetonitrile (20 mL) were added a solution of $AgBF_4$ (41 mg, 0.21 mmol) in acetonitrile (5 mL) and Et_3N (11 mg, 0.11 mmol). The solution was stirred for 3 h at 25 °C. Reduction of the solution volume gave white precipitate. It was collected, washed with methanol, and dried in vacuo. Yield: 78 mg (69%). It was recrystallized from $CHCl_3/CH_3OH$.

*[Pt_2Ag_4(μ-Me_2pz)$_2$(μ-Ph_2pz)$_6$] (**8**).* To a solution of **6** (105 mg, 0.11 mmol) in acetonitrile (20 mL) were added Et_3N (23 mg, 0.23 mmol) and a solution of $AgBF_4$ (45 mg, 0.23 mmol) in acetonitrile (10 mL). The solution was stirred for 3 h at 25 °C. Reduction of the solution volume gave white precipitate. It was collected, washed with methanol, dried in vacuo, and then recrystallized from $CHCl_3/CH_3OH$. Yield 26 mg (21%). Anal. Calcd for $C_{100}H_{80}Ag_4N_{16}Pt_2$: C, 51.61; H, 3.46; N, 9.63. Found: C, 51.39; H, 3.32; N, 9.54. ^{1}H NMR (300 MHz, $CDCl_3$, 25 °C, TMS): δ = 7.39−6.71 (m, 56H, Ph), 6.38 (d, J = 2.4 Hz, 4H, Ph), 6.35 (d, J = 2.2 Hz, 2H, H_4 of Ph_2pz), 5.99 (d, J = 2.5 Hz, 2H, H_4 of Ph_2pz), 5.84 (d, J = 2.5 Hz, 2H, H_4 of Ph_2pz), 4.83 (d, J = 2.3 Hz, 2H, H_4 of Me_2pz), 1.52 (s, 6H, Me), 1.26 ppm (s, 6H, Me).

X-ray Structural Determinations. Crystals suitable for X-ray structural analysis were obtained by recrystallization from CH_2Cl_2/CH_3OH (**2**·CH_3OH, **3**·$3CH_2Cl_2$), $CHCl_3/CH_3CN$ (**4**·$2CH_3CN$, **5**·$2CH_3CN$), and $CHCl_3/CH_3OH$ (**7**·$0.5CH_3OH$·$0.5H_2O$, **8**), respectively. The crystal of **7**·$0.5CH_3OH$·$0.5H_2O$, and **8** were mounted on a glass fiber, while the crystals, **2**·CH_3OH, **3**·$3CH_2Cl_2$, **4**·$2CH_3CN$, and **5**·$2CH_3CN$ were sealed in thin-walled glass capillaries. Intensity data were collected on a Mercury CCD area detector coupled with a Rigaku AFC7S diffractometer using graphite-monochromated Mo Kα (λ = 0.71070 Å) radiation at 296 K. Final cell parameters were obtained from a least-squares analysis of reflections with $I > 10\sigma(I)$. The data were corrected for Lorentz and polarization effects. An empirical absorption correction was applied.[34] We have noticed a low completeness of data collection for **7**·$0.5CH_3OH$·$0.5H_2O$ during structural analysis, we have not succeeded in preparing another crystals suitable for X-ray structural analysis.

The crystal structures of **2**·CH_3OH and **5**·$2CH_3CN$ were solved by direct method (SIR92).[35] Those of **3**·$3CH_2Cl_2$, **4**·$2CH_3CN$, **7**·$0.5CH_3OH$·$0.5H_2O$, and **8** were solved by heavy-atom method by using DIRDIF.[36] The positional and thermal parameters of non-H atoms were refined anisotropically by the full-matrix least-squares method. The minimized function was $\Sigma w(F_o^2 - F_c^2)^2$. Hydrogen atoms were included at calculated positions with fixed displacement parameters except for the hydrogen atoms in Ph_2pzH ligands participating in the hydrogen bonding in **2**·CH_3OH. In the final cycle of the refinement, parameter shifts were less than 0.1σ. No correction was made for secondary extinction.

All calculations were performed using the CrystalStructure[37] crystallographic software package except for refinement, which was performed using SHELXL-97.[38] Further crystallographic data are given in Table 3. Listings of the selected bond distances and angles are summarized in Supporting Information Tables S1−S6.

Computational Methods. The geometries of **3**, **4**, **5**, **7**, and **8** were optimized with the DFT method, where B3LYP functional was employed.[39−41] X-ray structures were used as initial geometries without any geometrical constraints. In these calculations, for all metals, basis sets with ECPs proposed by Christiansen et al were employed.[42−44] In details, for Cu, Ag, and Pt atoms, (761/6711/411), (541/541/211), and (541/5511/211) basis sets were used, respectively. For Cl, C, N, and H atoms, usual cc-pVDZ basis sets were used.[45,46] All calculations were carried out using the Gaussian 03 package.[47] Molecular orbitals with the isovalue of 0.02 were drawn by the Gauss View 4.1.[48]

■ ASSOCIATED CONTENT

Ⓢ Supporting Information

Characterization of intermediate species, crystallographic data, and tables of selected bond lengths and angles for **2**·CH_3OH, **3**·$3CH_2Cl_2$, **4**·$2CH_3CN$, **5**·$2CH_3CN$, **7**·$0.5CH_3OH$·$0.5H_2O$, and **8**, optimized geometries, special plot of selected molecular orbitals for **5**, excitation, emission and diffuse reflectance spectra of **3**, **4**, **7**, and **8**, emission spectra of **6**, VT NMR spectra of **2**, ^{1}H NMR spectra of the intermediate species with related complexes, and crystal structures of **3**, **4**, **5**, **7**, and **8**. This material is available free of charge via the Internet at http://pubs.acs.org.

■ AUTHOR INFORMATION

Corresponding Author

*E-mail: kumks@nagasaki-u.ac.jp.

Notes

The authors declare no competing financial interest.

■ ACKNOWLEDGMENTS

This work was partially supported by a Grant-in-Aid for Scientific Research (No. 21550062).

■ REFERENCES

(1) Espinet, P.; Forniés, J.; Martinez, F.; Tomás, M.; Lalinde, E.; Moreno, M. T.; Ruiz, A.; Welch, A. J. *J. Chem. Soc., Dalton Trans.* **1990**, 791−798.

(2) Yam, V. W.-W.; Yu, K.-L.; Cheung, K.-K. *J. Chem. Soc., Dalton Trans.* **1999**, 2913−2915.

(3) Charmant, J. P. H.; Forniés, J.; Gómez, J.; Lalinde, E.; Merino, R. I.; Moreno, M. T.; Orpen, A. G. *Organometallics* **1999**, *18*, 3353−3358.

(4) Ara, I.; Forniés, J.; Gómez, J.; Lalinde, E.; Moreno, M. T. *Organomeistallics* **2000**, *19*, 3137−3144.

(5) Yam, V. W.-W.; Hui, C.-K.; Yu, S., -Y.; Zhu, N. *Inorg. Chem.* **2004**, *43*, 812−821.

(6) Forniés, J.; Fuertes, S.; Martín, A.; Sicilia, V.; Lalinde, E.; Moreno, M. T. *Chem.—Eur. J.* **2006**, *12*, 8253−8266.
(7) Gil, B.; Forniés, J.; Gómez, J.; Lalinde, E.; Martín, A.; Moreno, M. T. *Inorg. Chem.* **2006**, *45*, 7788−7798.
(8) Leung, S. Y.-L.; Lam, W. H.; Zhu, N.; Yam, V. W.-W. *Organometallics* **2010**, *29*, 5558−5569.
(9) Chen, Z.-N.; Zhao, N.; Fan, Y.; Ni, J. *Coord. Chem. Rev.* **2009**, *253*, 1−20.
(10) Díez, Á.; Lalinde, E.; Moreno, M. T. *Coord. Chem. Rev.* **2011**, *255*, 2426−2447.
(11) Berenguer, J. R.; Lalinde, E.; Moreno, M. T. *Coord. Chem. Rev.* **2010**, *254*, 832−875.
(12) Berenguer, J. R.; Forniés, J.; Gómez, J.; Lalinde, E.; Moreno, M. T. *Organometallics* **2001**, *20*, 4847−4851.
(13) Fernández, J.; Forniés, J.; Gil, B.; Gómez, J.; Lalinde, E.; Moreno, M. T. *Organometallics* **2006**, *25*, 2274−2283.
(14) Berenguer, J. R.; Forniés, J.; Gil, B.; Lalinde, E. *Chem.—Eur. J.* **2006**, *12*, 785−795.
(15) Berenguer, J. R.; Gil, B.; Fernández, J.; Forniés, J.; Lalinde, E. *Inorg. Chem.* **2009**, *48*, 5250−5262.
(16) Forniés, J.; Fuertes, S.; Martin, A.; Sicilia, V.; Gil, B.; Lalinde, E. *Dalton Trans.* **2009**, 2224−2234.
(17) Berenguer, J. R.; Fernández, J.; Gil, B.; Lalinde, E.; Sánchez, S. *Inorg. Chem.* **2010**, *49*, 4232−4244.
(18) Berenguer, J. R.; Díez, A.; Fernndez, J.; Forniés, J.; García, A.; Gil, B.; Lalinde, E.; Moreno, M. T. *Inorg. Chem.* **2008**, *47*, 7703−7716.
(19) Shavaleev, N. M.; Accorsi, G.; Virgili, D.; Bell, Z. R.; Lazarides, T.; Calogero, G.; Armaroli, N.; Ward, M. D. *Inorg. Chem.* **2005**, *44*, 61−72.
(20) Ward, M. D. *Coord. Chem. Rev.* **2007**, *251*, 1663−1677.
(21) Xu, H.-B.; Zhang, L.-Y.; Xie, Z.-L.; Ma, E.; Chen, Z.-N. *Chem. Commun.* **2007**, 2744−2746.
(22) Chen, Z.-N.; Fan, Y.; Ni, J. *Dalton Trans.* **2008**, 573−581.
(23) Li, X.-L.; Shi, L.-X.; Zhang, L.-Y.; Wen, H.-M.; Chen, Z.-N. *Inorg. Chem.* **2007**, *46*, 10892−10900.
(24) Xu, H.-B.; Ni, J.; Chen, K.-J.; Zhang, L.-Y.; Chen, Z.-N. *Organometallics* **2008**, *27*, 5665−5671.
(25) Xu, H.-B.; Zhang, L.-Y.; Chen, Z.-H.; Shi, L.-X.; Chen, Z.-N. *Dalton Trans.* **2008**, 4664−4670.
(26) Umakoshi, K.; Kojima, T.; Saito, K.; Akatsu, S.; Onishi, M.; Ishizaka, S.; Kitamura, N.; Nakao, Y.; Sakaki, S.; Ozawa, Y. *Inorg. Chem.* **2008**, *47*, 5033−5035.
(27) Umakoshi, K.; Saito, K.; Arikawa, Y.; Onishi, M.; Ishizaka, S.; Kitamura, N.; Nakao, Y.; Sakaki, S. *Chem.—Eur. J.* **2009**, *15*, 4238−4242.
(28) Calculated values in SciFinder using Advanced Chemistry Development (ACD/Laboratories) Software v11.02
(29) Ara, I.; Aranaz, J.; Forniés, J. *J. Fluorine Chem.* **2010**, *131*, 1103−1107.
(30) Albano, V. G.; Serio, M. D.; Monari, M.; Orabona, I.; Panunzi, A.; Ruffo, F. *Inorg. Chem.* **2002**, *41*, 2672−2677.
(31) The Ag···Cl distances are by 0.5 Å less than van der Wasls distance. However, the Cl−Pt−N(cis) angle is almost 90 degree and the Cl−Pt−N(trans) angle is 174 degree, which is almost linear, as seen in Table S3. If some coordination or covalent interaction exists between Ag and Cl atoms, the Pt−Cl moiety would distort from the planar geometry. It is likely that the rather short Ag···Cl distance arises from electrostatic interaction between Ag and Cl.
(32) Miskowski, V. M.; Houlding, V. H.; Che, C.-M.; Wang, Y. *Inorg. Chem.* **1993**, *32*, 2518−2524.
(33) Kukushkin, V. Y.; Oskarsson, Å.; Elding, L. I.; Jonasdottir, S. *Inorg. Synth.* **1997**, *31*, 279−284.
(34) Jacobson, R. A. *REQABS*, version 1.1; Molecular Structure Corp.: The Woodlands, TX, 1998.
(35) Altomare, A.; Cascarano, G.; Giacovazzo, C.; Guagliardi, A.; Burla, M. C.; Polidori, G.; Camalli, M. *J. Appl. Crystallogr.* **1994**, *27*, 435−436.
(36) Beurskens, P. T.; Admiraal, G.; Beurskens, G.; Bosman, W. P.; de Gelder, R.; Israel, R.; Smits, J. M. M. *The DIRDIF94 Program System*, Technical Report; Crystallography Laboratory, University of Nijmegen: The Netherlands, 1994.
(37) *CrystalStructure 4.0: Crystal Structure Analysis Package*; Rigaku Corporation: Tokyo, Japan, 2000−2010.
(38) Sheldrick, G. M. *Acta Crystallogr.* **2008**, *A64*, 112−122.
(39) Becke, A. D. *J. Chem. Phys.* **1992**, *96*, 2155−2160.
(40) Becke, A. D. *J. Chem. Phys.* **1993**, *98*, 5648−5652.
(41) Lee, C.; Yang, W.; Parr, R. G. *Phys. Rev. B* **1988**, *37*, 785−789.
(42) Hurley, M. M.; Pacios, L. F.; Christiansen, P. A.; Ross, R. B.; Ermler, W. C. *J. Chem. Phys.* **1986**, *84*, 6840−6850.
(43) LaJohn, L. A.; Christiansen, P. A.; Ross, R. B.; Atashroo, T.; Ermler, W. C. *J. Chem. Phys.* **1987**, *87*, 2812−2824.
(44) Ross, R. B.; Powers, J. M.; Atashroo, T.; Ermler, W. C.; LaJohn, L. A.; Christiansen, P. A. *J. Chem. Phys.* **1990**, *93*, 6654−6670.
(45) Woon, D. E.; Dunning, T. H. *J. Chem. Phys.* **1993**, *98*, 1358−1371.
(46) Dunning, T. H. *J. Chem. Phys.* **1989**, *90*, 1007−1023.
(47) Frisch, M. J.; Trucks, G. W.; Schlegel, H. B.; Scuseria, G. E.; Robb, M. A.; Cheeseman, J. R.; Montgomery, J. A. J.; Vreven, T.; Kudin, K. N.; Burant, J. C.; Millam, J. M.; Iyengar, S. S.; Tomasi, J.; Barone, V.; Mennucci, B.; Cossi, M.; Scalmani, G.; Rega, N.; Petersson, G. A.; Nakatsuji, H.; Hada, M.; Ehara, M.; Toyota, K.; Fukuda, R.; Hasegawa, J.; Ishida, M.; Nakajima, T.; Honda, Y.; Kitao, O.; Nakai, H.; Klene, M.; Li, X.; Knox, J. E.; Hratchian, H. P.; Cross, J. B.; Bakken, V.; Adamo, C.; Jaramillo, J.; Gomperts, R.; Stratmann, R. E.; Yazyev, O.; Austin, A. J.; Cammi, R.; Pomelli, C.; Ochterski, J. W.; Ayala, P. Y.; Morokuma, K.; Voth, G. A.; Salvador, P.; Dannenberg, J. J.; Zakrzewski, V. G.; Dapprich, S.; Daniels, A. D.; Strain, M. C.; Farkas, O.; Malick, D. K.; Rabuck, A. D.; Raghavachari, K.; Foresman, J. B.; Ortiz, J. V.; Cui, Q.; Baboul, A. G.; Clifford, S.; Cioslowski, J.; Stefanov, B. B.; Liu, G.; Liashenko, A.; Piskorz, P.; Komaromi, I.; Martin, R. L.; Fox, D. J.; Keith, T.; Al-Laham, M. A.; Peng, C. Y.; Nanayakkara, A.; Challacombe, M.; Gill, P. M. W.; Johnson, B.; Chen, W.; Wong, M. W.; Gonzalez, C.; Pople, J. A. *Gaussian 03*, revision C.02, Gaussian, Inc.: Wallingford CT, 2004.
(48) Dennington, R.; Keith, T.; William, J. *GaussView*, version 4.1, Gaussian, Inc.: Shawnee Mission, KS, 2007.

dx.doi.org/10.1021/ic202663q | *Inorg. Chem.* XXXX, XXX, XXX−XXX